Meteoritics & Planetary Science 37, 183–207 (2002)
Available online at http://www.uark.edu/meteor

A model of the thermal processing of particles in solar nebula shocks: Application to the cooling rates of chondrules

S. J. DESCH[1]* AND H. C. CONNOLLY, JR.[2]

[1]Department of Terrestrial Magnetism, Carnegie Institution of Washington, 5241 Broad Branch Road Northwest, Washington D.C. 20015, USA
[2]Kingsborough College-CUNY, Department of Physical Sciences, 2001 Oriental Boulevard, Brooklyn, New York 11235, USA
*Correspondence author's e-mail address: desch@dtm.ciw.edu

(Received 2001 August 28; accepted in revised form 2001 October 31)

Abstract–We present a model for the thermal processing of particles in shock waves typical of the solar nebula. This shock model improves on existing models in that the dissociation and recombination of H_2 and the evaporation of particles are accounted for in their effects on the mass, momentum and energy fluxes. Also, besides thermal exchange with the gas and gas-drag heating, particles can be heated by absorbing the thermal radiation emitted by other particles. The flow of radiation is calculated using the equations of radiative transfer in a slab geometry. We compute the thermal histories of particles as they encounter and pass through the shock.

We apply this shock model to the melting and cooling of chondrules in the solar nebula. We constrain the combinations of shock speed and gas density needed for chondrules to reach melting temperatures, and show that these are consistent with shock waves generated by gravitational instabilities in the protoplanetary disk. After their melting, cooling rates of chondrules in the range 10–1000 K h^{-1} are naturally reproduced by the shock model. Chondrules are kept warm by the reservoir of hot shocked gas, which cools only as fast as the dust grains and chondrules themselves can radiate away the gas's energy. We predict a positive correlation between the concentration of chondrules in a region and the cooling rates of chondrules in that region. This correlation is supported by the unusually high frequency of (rapidly cooled) barred chondrules among compound chondrules, which must have collided preferentially in regions of high chondrule density. We discuss these and other compelling consistencies between the meteoritic record and the shock wave model of chondrule formation.

INTRODUCTION

Chondrules—tiny (diameters 0.1–1 mm), igneous spheres of ferromagnesian silicates—make up more than half of all the meteoritic material that falls to Earth each year (see Hewins, 1996 and articles therein). The asteroid belt probably contains over 10^{24} g of chondrules (Levy, 1988), each one of which was melted during the first 10 Ma of the solar system (Swindle *et al.*, 1996). While rare presolar grains exist (Zinner, 1997), chondrules and calcium-aluminum-rich inclusions (CAIs), also found in carbonaceous chondrites, are the oldest rocks formed in the solar system. Of all meteoritic material, chondrules and CAIs have the most to tell us about the conditions in the solar nebula: what were the gas pressures, temperatures and compositions, what was the role of turbulence, and what energetic processes were taking place in the solar nebula to melt the chondrules. Probably no problem is as fundamental to meteoritics as the problem of how chondrules formed and were melted. Yet, despite the discovery of chondrules exactly 200 years ago by Howard and de Bournon (Howard, 1802; Wood, unpubl. data), the first proposal of a chondrule formation theory 125 years ago (Sorby, 1877), and an explosion of progress in the last several decades, no theory of chondrule formation enjoys widespread acceptance. The state of the field was reviewed by Boss (1996) and Wood (unpubl. data).

Some proposed models of chondrule formation involve melting chondrules near the early Sun, by sunlight and radiation associated with flares (Shu *et al.*, 1996, 2001), or by ablation of planetesimals in a bipolar outflow (Liffman and Brown, 1996). The newly melted chondrules are then injected into the present-day asteroid belt region by the hypothesized x-wind (Shu *et al.*, 2001), or a bipolar outflow (Liffman and Brown, 1996), and sent on ballistic trajectories into the protoplanetary disk. In both models, smaller (~1 μm) dust particles would necessarily follow trajectories different from those of chondrules. None of the above models has calculated detailed thermal histories of any particles, and have not yet been demonstrated to match cooling rates of chondrules ("Thermal Histories"). We also note that generally, the chondrules that are most opaque at visible wavelengths (the type I, FeO-poor

Prelude preprint MS#4636

chondrules, because they contain metal; McSween, 1977) experienced less heating than the metal-poor, type II FeO-rich chondrules (Hewins, 1997), arguing against melting by optical radiation. Moreover, the two models above are contrary to the following lines of evidence that chondrules formed in the same environment as the dust grains that surround the chondrules and make up chondritic matrix. First, while chondrules and the matrix grains are each compositionally distinct from a solar (CI) composition, the combined chondrules and matrix are together quite close to solar composition, in Murchison (Wood, 1985), Allende (Palme *et al.*, 1993), and in ordinary chondrites (Huss, 1988). This implies that chondrules and matrix grains within a given chondrite are derived from the same batch of solar composition material. Second, many chondrules have rims of dust grains that they accreted after they melted. The thicknesses of these rims are correlated with the size of the chondrules, in a way that is consistent with chondrules depleting all of the dust in a local environment (Morfill *et al.*, 1998), but is not consistent with injection of chondrules into a dusty region from an outside region (such as the Sun) without fine-tuning of the dust-to-gas ratio (Liffman and Toscano, 2000).

Among models of chondrule formation in the solar nebula are lightning (Whipple, 1966; Pilipp *et al.*, 1998; Desch and Cuzzi, 2000) and nebular shocks (Wood, 1963, 1984, 1996; Hood and Horanyi, 1991, 1993; Ruzmaikina and Ip, 1994; Connolly and Love, 1998). Lightning is plausibly generated in a turbulent solar nebula (Desch and Cuzzi, 2000), and is capable of melting chondrules, either by heating from the discharge itself (Horanyi and Robertson, 1996), or by heating a large volume of gas, which then melts the chondrules (Desch, 2000). The cooling rates of chondrules have not been reproduced in detail, but are estimated to be comparable to those of observed chondrules (Desch, 2000). Wasilewski and Dickinson (2000) have argued that the remanent magnetization of some Bjurbole (LL4) chondrules probably cannot be explained by any mechanism *other* than lightning (including contamination by a standard hand magnet). Thus, lightning remains a plausible chondrule formation mechanism, although the details of lightning generation, relying on not-well-constrained properties of triboelectric charging and electric discharge, prevent firm predictions of how lightning would form and melt chondrules.

Much better understood are shock waves in the solar nebula. Shock waves could conceivably be produced in a number of nebular environments, including: accretion shocks (Wood, 1984; Ruzmaikina and Ip, 1994); bow shocks from planetesimals in eccentric orbits (Hood, 1998; Weidenschilling *et al.*, 1998); tidal interactions with passing stars (Larson, 2002); infalling clumps (Boss and Graham, 1993; Tanaka *et al.*, 1998); and spiral density waves (Wood, 1996) or other global gravitational instabilities (Boss, 2000). It has been shown that (normal) velocities of chondrules relative to shocks in the solar nebula ~6 km s^{-1} are sufficient to melt chondrules (Hood and Horanyi, 1993; Connolly and Love, 1998; Ciesla and Hood, 2001; Desch and Connolly, 2001). As this is only a fraction of the orbital velocity (~19 km s^{-1}) of particles at 2.5 AU, where chondrules are found today, nebular shocks plausibly could reach the strengths needed to melt chondrules. Unfortunately, numerical simulations of solar nebula hydrodynamics lack the resolution yet to quantify where, and when in the solar nebula's evolution, shocks would occur, and with what strengths. Despite general agreement between shock heating and the petrology of chondrules (Connolly and Love, 1998), the lack of a repeatable shock source has hindered acceptance of the nebular shock wave model for chondrule formation (*e.g.*, Boss, 1996).

What is hindering acceptance of the shock model even more, though, is the perceived inability of shocks to match the cooling rates of chondrules (*e.g.*, Wasson, 1993; Jones *et al.*, 2000). Chondrules' cooling rates are inferred from their textures and chemical zoning in their phenocrysts to be in the range 5–3000 K h^{-1} (see "Thermal Histories, Chondrules"). Chondrules therefore took hours to days to cool. Type B, type C and compact type A CAIs were also melted, and the texture and chemical zoning in the melilite of type B CAIs constrains the cooling rates of these CAIs to be 0.5–50 K h^{-1}. We view it as likely that chondrules and CAIs were melted by the same mechanism. Chondrules that radiate away their internal heat energy to free space cool in less than a second, at rates ~3×10^6 K h^{-1}. Therefore chondrules either did not radiate to free space and were immersed in an optically thick environment, or were continually heated as they radiated, or both. Nebula shocks would heat chondrules in their paths because the shock would instantaneously (<< milliseconds) accelerate nebula gas to velocities ~10 km s^{-1}, while the chondrules and other solid particles would take longer to come up to speed with the gas. The aerodynamic response time (stopping time) in solar nebula gas for particles smaller than 1 cm in diameter is given by

$$t_{\rm stop} = \frac{\rho_{\rm p} a_{\rm p}}{\rho_{\rm g} C_{\rm s}} \qquad (1)$$

where $\rho_{\rm p}$ and $a_{\rm p}$ are the material density and radius of the particle, and $\rho_{\rm g}$ and $C_{\rm s}$ are the density and sound speed of the (post-shock) gas (Cuzzi *et al.*, 1996). Typical timescales for particle and gas velocities to match are seconds to minutes, during which time the friction of the gas supersonically passing the particles heats them ("gas-drag heating"), even melting them. The misconception that shocks cannot explain chondrule cooling rates (*e.g.*, Wasson, 1993; Jones *et al.*, 2000) stems from the assumption that chondrules are heated *only* by frictional heating. Since frictional heating vanishes once the chondrules and gas match velocities, the chondrule temperature must decrease over a timescale $t_{\rm stop}$. Stopping times of hours are achieved only in very low-density gas (*post*-shock density <10^{-10} g cm^{-3}), for which only exceptionally high velocities, ~30 km s^{-1}, (much greater than the orbital velocities at 2.5 AU) will melt chondrules (*e.g.*, Ruzmaikina and Ip, 1994). For plausible nebula models, the post-shock gas density is at least 10^{-9} g cm^{-3} and the shock velocities probably <10 km s^{-1}, so

the observed cooling of chondrules over hours timescales implies that chondrules were not continuously heated by gas-drag heating alone while radiating to free space.

Most shock models today therefore assume that chondrules heated by shocks are immersed in an optically thick environment that slows the escape of radiation energy from the region, preventing chondrules from cooling (Sahagian and Hewins, 1992; Hood and Horanyi, 1993; Hood and Kring, 1996; Hood and Ciesla, 2001). In contrast to the conclusions of these authors, however, we find that even an optically thick slab will cool rapidly. We take the example of Sahagian and Hewins (1992), a 1000 km thick slab of chondrules with radii $a_p \approx 420\ \mu$m and spatial mass density $\rho = 10^{-8}$ g cm^{-3}, in which the heat capacity of the gas is negligible. The timescale for radiative diffusion to allow relaxation of a temperature fluctuation in this slab is

$$t_{rd} = \frac{\rho C_P \lambda}{16\sigma T_0^3}\left[1-\left(\frac{L}{2\pi\lambda}\right)\cot^{-1}\left(\frac{L}{2\pi\lambda}\right)\right]^{-1} \rightarrow \frac{3\rho C_V L^2}{64\pi^2\lambda\sigma T_0^3} \quad (2)$$

(Spiegel, 1972; Mihalas and Mihalas, 1985), where the last expression is t_{rd} in the limit $L >> \lambda$ of large optical depth (Kippenhahn and Weigert, 1990). In this example: $\rho = 10^{-8}$ g cm^{-3} is the spatial mass density of chondrules; $C_P \approx 10^7$ erg g^{-1} K^{-1} is the heat capacity of the chondrule material; σ is the Stefan–Boltzmann constant; $\lambda = 180$ km is the mean free path of photons in the chondrule region; $L \approx 500$ km is the lengthscale associated with the temperature disturbance; and $T_0 \approx 1500$ K is the chondrule temperature at which the cooling rates are relevant. The cooling timescale thus derived is ~0.6 s in the limit $L = 0$ (radiating to free space), and 1.2 s for $L = 500$ km. Cooling timescales of 1 h are obtained only when $L \approx 10^5$ km, equivalent to a column density of chondrules $\gtrsim$100 g cm^{-2}. The addition of a mass of fine-grained dust equal in mass to the chondrules, but with $a_p = 0.3\ \mu$m (and emissivity 0.2; see "Shock Code, Inputs"), would increase the cooling timescale to only 24 s (cooling rates ~10^5 K h^{-1}) for $L = 500$ km, using a column density of dust and chondrules of 1.0 g cm^{-2}. To explain chondrule cooling rates of even 10^3 K h^{-1} would require a column density of dust and chondrules $\gtrsim$8 g cm^{-2}, and cooling rates of porphyritic chondrules, 10^2 K h^{-1} require another factor of 3 increase in solids column density, to 24 g cm^{-2}. If the cooling rates are actually closer to 10 K h^{-1}, then even more solids need to be heated. For comparison, the *total* column density of solids at 2.5 AU in the "minimum-mass" nebula is only 1.8 g cm^{-2} (Hayashi, 1981), and even in our preferred model of a massive disk, the total column density of solids is ~10^2 g cm^{-2}. For a solar gas-to-solids ratio and gas density ~10^{-9} g cm^{-3}, column densities of 24 g cm^{-2} are achieved only on lengthscales ~5×10^7 km, comparable to the scale height of the nebula. If the slow cooling rates of chondrules are to be explained by trapping of thermal radiation, extremely large regions the size of the nebula must be heated, and heated simultaneously in less than the cooling time of several hours ($\lesssim 10^5$ s). The trigger for this instantaneous heating would have to sweep through the region at speeds ~10^3 km s^{-1} for this scenario to occur. Trapping of radiation is highly unlikely to have any effect on the cooling rates of chondrules for the parameters we consider relevant to chondrule formation. While absorption of other chondrules' thermal emissions will increase the peak temperatures of chondrules ("Results, Effects of Radiation and Dissociation"), in terms of the cooling rate chondrules might as well be radiating to free space. As argued by Desch (2000), the slow cooling rates of chondrules *must* be due to their immersion in the hot, post-shock gas, which itself is slowly cooling. Wasson (1996) has similarly argued that when chondrules are heated, a comparable mass of gas, with its much higher heat capacity, will also be heated, and this hot gas will dominate the thermal evolution of the system.

We present new numerical simulations of the melting of chondrules (and type B CAIs) as they pass through a solar nebula shock (Desch and Connolly, 2001). We include a separate calculation of the gas energetics, and the effects of hydrogen dissociation and recombination. We also account for the transfer of radiation for the first time. (Ruzmaikina and Ip (1994) allowed chondrules to cool by radiation and to absorb radiation emitted by the gas, but chondrules did not absorb radiation from other chondrules. Hood and Horanyi (1993) assumed optically thick jump conditions immediately across the shock front, and allowed chondrules to absorb radiation from other chondrules only within a 200 km radius sphere.) We also allow for the evaporation of particles and the interaction between particles and gas this would cause. We show that when these new physical effects are included in the shock wave model, as they must be, the predicted thermal histories of chondrules (and type B CAIs) during melting and cooling agree in detail with their thermal histories as inferred from petrologic observations.

THERMAL HISTORIES

Chondrules

Constraints can be placed on the petrogenesis of chondrules and type B CAIs by measurements of the elemental distributions within individual crystals, crystal morphology, and overall textures compared with experimental analogs. The thermal histories of chondrules, both before and immediately after their melting, are constrained by the presence of volatile and moderately volatile elements such as S and Na in them. *If* chondrules inherited these elements from their precursors, and *if* these precursors equilibrated with their surroundings, then it is required that chondrules achieved peak melting temperatures rapidly ("flash melting"), since prolonged heating before peak melting, and at peak melting temperature, promotes the evaporation of such elements. Sulfur, which is usually observed as troilite, an iron-sulfide, volatilizes above 650 K (for total pressures of 10^{-6} bar; Jones *et al.*, 2000); thus if troilite in chondrules was derived from S that was present within

chondrule precursors, those precursors could not have experienced prolonged heating above 650 K before or during melting. Sulfur in chondrules may be primary (*i.e.*, present in the chondrule precursors), or secondary, arriving in chondrules after their formation due to gas-solid exchange while the chondrules were free in the nebula, or later exchange processes when the chondrules were in their parent bodies. Rubin *et al.* (1999) tested whether the sulfide within chondrules from ordinary chondrites was primary, based on textural evidence such as whether troilite was located near the chondrule centers and whether the troilite was completely embedded in a mafic silicate. Based on these criteria, Rubin *et al.* (1999) concluded that at least 13% of the chondrules they surveyed contained troilite that is primary; no conclusions could be made about the other 87% of chondrules. Since S was originally within the same fraction of chondrule precursors (potentially as troilite), the ambient temperature of the nebula was probably below 650 K.

Constraints can also be applied to the melting process, although it must be remembered that melting is a kinetic process, far from equilibrium. Because a brief and intense melting event can mimic a prolonged but moderate melting event, the duration of melting is intimately associated with the peak temperatures achieved during melting. Chondrules appear to have been almost completely melted for timescales of minutes. Chondrule analogs heated for <1 s are texturally different from real chondrules (Hewins *et al.*, 2000), because thermal diffusion within a chondrule takes a fraction of a second (Horanyi and Robertson, 1996). The minimum timescale for melting imposes a maximum temperature so that crystallization nuclei are preserved. Chondrules with barred and radial textures had to be completely melted, so that all crystallization nuclei were destroyed, whereas porphyritic textures are produced when some nuclei remain. Hewins and Connolly (1996) found in their experiments that for short durations of heating (5 min), porphyritic olivine textures require peak temperatures 80–120 °C, and barred olivine textures 150–400 °C above their respective liquidus temperatures. The most refractory chondrules have liquidus temperatures over 1750 °C, and so at least some chondrules experienced peak temperatures of over 1850 °C (2120 K), at least for a few minutes. Considering the range of liquidus temperatures and textures, a range of peak temperatures 1500–1850 °C (1770–2120 K), which chondrules experienced for minutes, is inferred (Hewins and Connolly, 1996).

After this initial peak temperature, the chondrule cools. Despite the common experimental practice of assuming a constant (linear) cooling rate, the cooling rate almost certainly varied with temperature. We distinguish between cooling from the peak temperature down to the liquidus, and cooling through the crystallization temperature range down to the solidus. Retention of S during heating was studied by Yu *et al.* (1996) and Yu and Hewins (1998), who found that at least 10% of primary S could be retained in type IIAB chondrule analogs, even when heated to temperatures 250 °C above their liquidi, provided *initial* cooling rates were comparable to at least 5000 K h^{-1} through the liquidus temperature. Cooling rates in these experiments subsequently fell to a few $\times 10^2$ K h^{-1} in the crystallization temperature range. Constraints on cooling rates are much more extensive in the crystallization temperature range (about 1100–1400 °C for type IIA PO chondrules (Radomsky and Hewins, 1990)), and are imposed by the textures and chemical zoning of chondrules' phenocrysts (large crystals). The most often quoted cooling rates of chondrules are 50–1000 K h^{-1}; the cooling rates of CAIs (see "Thermal Histories, Calcium-Aluminum-Rich Inclusions") can only be constrained for type B CAIs, for which the cooling rates are 0.5–50 K h^{-1} (Jones *et al.*, 2000). The lack of overlap in the cooling rates has been used to argue that chondrules and igneous CAIs were melted by different processes, but a review of literature suggests that overlap does exist between type B CAIs and porphyritic chondrules. Tables 1–3 list the results of several experiments on chondrule analogs, ordering them by texture produced. The textures are abbreviated as follows: an initial "P" stands for porphyritic, a "B" stands for barred, an "R" for radial, and a "G" for granular. The following letters indicate whether the chondrule is olivine-rich ("O"), pyroxene-rich ("P"), or has both minerals ("OP" or "PO"). Glassy chondrules, which do not contain crystalline minerals, are denoted "GL". The compositions are classified as follows (McSween, 1977): type I refers to FeO-poor chondrules, type II to FeO-rich, type III to silica rich; "A" refers to <10 modal percent pyroxene, "AB" refers to between 10 and 90 modal percent pyroxene, and "B" refers to >90 modal percent pyroxene (as opposed to olivine). The references are: (1) Connolly and Hewins (1991); (2) Connolly and Hewins (1995); (3) Connolly *et al.* (1998); (4) DeHart and Lofgren (1996); (5) Hewins *et al.* (1981); (6) Jones and Lofgren (1993); (7) Kennedy *et al.* (1993); (8) Lofgren (1989); (9) Lofgren and Lanier (1990); (10) Lofgren and Russell (1986); (11) Radomsky and Hewins (1990); (12) Weinbruch and Muller (1995); (13) Weinbruch *et al.* (1998). Some experiments compared textures only, while some compared textures and chemical zoning simultaneously; we consider the latter the most reliable studies and use them to make the following statements. Radial-textured chondrules (olivine or pyroxene-rich) cooled at rates 5–3000 K h^{-1} (Lofgren and Russell, 1986). Barred olivines cooled at rates 500–3000 K h^{-1} (Connolly *et al.*, 1998, based on textures alone). The 85% of all chondrules that have porphyritic olivine textures (Gooding and Keil, 1981) cooled at rates 5–100 K h^{-1} (at least for type IIA analogs; Jones and Lofgren, 1993). Granular olivine/pyroxene chondrules, a subset of porphyritic chondrules, likely cooled at slower cooling rates <100 K h^{-1}, but detailed chemical studies of these chondrules are limited. A typical cooling rate of ~40 K h^{-1} corresponds to chondrules being partially molten for ~10 h. This is not inconsistent with the growing evidence that chondrules may have experienced evaporation and open-system behavior during their melting (Sears *et al.*, 1996; Cohen *et al.*, 2000). We also note that cooling rates ~40 K h^{-1} at temperatures above the liquidus are

TABLE 1. Experimental cooling rates of porphyritic chondrules.

Text. type	Comp. type	Melt time (min)	Melting temperature	Cooling rate (K/h)	Nucleating temperature	Constraint	Reference*
PO	IA	30	At, below T_{liq}	100–1000	Far below T_{liq}	Texture, zoning	11
PO	IA	30	Below T_{liq}	10–30	Below T_{liq}	Mesostasis comp., TL	4
PO	IAB, IIA	30	Above, down to T_{liq}	500	Near, below T_{liq}	Texture	2
PO	IIA	120–180	Below T_{liq}	5–100	Below T_{liq}	Texture, zoning	6
PO	IIA	120	Below T_{liq}	5–1000	Below T_{liq}	Texture, chemistry	8
PO	IIA	30	Below T_{liq}	500	Below T_{liq}	Texture	1
POP	IIAB	30	From above T_{liq}	500	Near T_{liq}	Texture	2
POP	IAB	30	Below T_{liq}	10–100	Below T_{liq}	Texture	11
POP	IIAB	1000	Below T_{liq}	5–2500	Below T_{liq}	Texture	10
POP	IIAB	?	Near T_{liq}	10–2000	Below T_{liq}	Texture, chemistry	13
PP	IIB?	1000	Below T_{liq}	5–100	Below T_{liq}	Texture, chemistry	7
PPO	IIAB	30	Below T_{liq}	500	Below T_{liq}	Texture	2

*References: (1) Connolly and Hewins (1991); (2) Connolly and Hewins (1995); (3) Connolly *et al.* (1998); (4) DeHart and Lofgren (1996); (5) Hewins *et al.* (1981); (6) Jones and Lofgren (1993); (7) Kennedy *et al.* (1993); (8) Lofgren (1989); (9) Lofgren and Lanier (1990); (10) Lofgren and Russell (1986); (11) Radomsky and Hewins (1990); (12) Weinbruch and Muller (1995); (13) Weinbruch *et al.* (1998).
Abbreviations: PO = porphyritic olivine, POP = porphyritic olivine-pyroxene, PP = porphyritic pyroxene, TL = thermoluminescence.

TABLE 2. Experimental cooling rates of barred, radial chondrules.

Text. type	Comp. type	Melt time (min)	Melting temperature	Cooling rate (K/h)	Nucleating temperature	Constraint	Reference*
BO	IIA	120	Above T_{liq}	1000–3000	Near T_{liq}	Texture	8
BO	IIA	120	Near T_{liq}	1000–3000	Near T_{liq}	Texture, bar width	9
BO	IIAB	30	Near T_{liq}	250–1000	Near T_{liq}	Texture	11
BO	II	<8	Above T_{liq}	500	Near T_{liq}	Texture	3
BO	IAB	30	Above T_{liq}	500	Near T_{liq}	Texture	2
BO/POP	IIA	30	Below T_{liq}	500	Below T_{liq}	Texture	2
BP	IAB	30	Above T_{liq}	500	Near T_{liq}	Texture	2
RP	IIB, III?	1000	Above, just below T_{liq}	5–3100	Unknown	Texture only	10
RP	III?	120	At T_{liq}	50–3000	Unknown	Texture, chemistry	5
RPO	IIA, IIAB	30	Above T_{liq}	500	Far below T_{liq}	Texture	2

*References: (1) Connolly and Hewins (1991); (2) Connolly and Hewins (1995); (3) Connolly *et al.* (1998); (4) DeHart and Lofgren (1996); (5) Hewins *et al.* (1981); (6) Jones and Lofgren (1993); (7) Kennedy *et al.* (1993); (8) Lofgren (1989); (9) Lofgren and Lanier (1990); (10) Lofgren and Russell (1986); (11) Radomsky and Hewins (1990); (12) Weinbruch and Muller (1995); (13) Weinbruch *et al.* (1998).
Abbreviations: BO = barred olivine, POP = porphyritic olivine-pyroxene, BP = barred pyroxene, RP = radial pyroxene, RPO = radial porphyritic-olivine.

inconsistent with retention of primary S (Yu *et al.*, 1996) and preservation of crystallization nuclei (Lofgren and Lanier, 1990; Radomsky and Hewins, 1990; Lofgren and Le, 1996). The textural and chemical evidence is saying that chondrules cooled off very rapidly (>5000 K h^{-1}) just above the liquidus, and slowly (5–3000 K h^{-1}) at temperatures between the liquidus and solidus.

Calcium-Aluminum-Rich Inclusions

Calcium-aluminum-rich inclusions are also termed refractory inclusions because the CAI precursors were composed of mineral phases that are the first to condense out of a cooling gas of solar composition, although it should be remembered that CAIs typically have lower melting points than many chondrules. CAIs are subclassified into three categories—A, B and C—on the basis of their mineral compositions. Of these, all but a subset of type A CAIs (the "fluffy" type As) show unequivocal evidence of having been melted (MacPherson *et al.*, 1988). It is this melting stage, and not any earlier stage of thermal processing experienced by CAIs, that we seek to model by shocks. The only constraints on thermal histories of CAIs (during the melting event) exist for type Bs. Their igneous textures can be reproduced experimentally only if the melilite

TABLE 3. Experimental cooling rates of other chondrules.

Text. type	Comp. type	Melt time (min)	Melting temperature	Cooling rate (K/h)	Nucleating temperature	Constraint	Reference*
GO	IIAB	30	Far below T_{liq}	500	Far below T_{liq}	Texture	11
GO	IIA	<8	Far below T_{liq} (flash)	500	Far below T_{liq}	Texture	3
GO	IIA	30	Far below T_{liq}	500	Far below T_{liq}	Texture	11
GOP	IAB?	N/A	N/A	3–30	N/A	Pyroxene chemistry	12
GL	IA, IIAB	30	Above T_{liq}	10–1000	None	Texture	11
GL	IIAB	30	Above T_{liq}	500	None	Texture	2
GL	IIA	30	Above T_{liq}	500	None	Texture	1
GL	III	< 8	Above T_{liq}	500	None	Texture	3

*References: (1) Connolly and Hewins (1991); (2) Connolly and Hewins (1995); (3) Connolly *et al.* (1998); (4) DeHart and Lofgren (1996); (5) Hewins *et al.* (1981); (6) Jones and Lofgren (1993); (7) Kennedy *et al.* (1993); (8) Lofgren (1989); (9) Lofgren and Lanier (1990); (10) Lofgren and Russell (1986); (11) Radomsky and Hewins (1990); (12) Weinbruch and Muller (1995); (13) Weinbruch *et al.* (1998). Abbreviations: GO = granular olivine, GOP = granular olivine-pyroxene, GL = glass.

appearance temperature is not exceeded by more than a few tens of degrees Kelvin. This places an upper limit of ~1425 °C (1700 K) on the temperatures these CAIs experienced (Stolper and Paque, 1986). In the experiments of Stolper and Paque (1986), the CAI analogs were held at the maximum temperatures for 3 h, giving the objects time enough to equilibrate. Shorter or longer (perhaps much longer) timescales may have occurred, but there are no constraints. Unlike chondrules, CAIs are not rich in volatile or moderately volatile elements, again making it difficult to constrain the maximum duration of melting. The cooling rates of type B CAIs fall in the range 0.5–50 K h^{-1}, with the slower end tending to reproduce more objects more analogous to real CAIs (Stolper and Paque, 1986; Jones *et al.*, 2000 and references therein). This constraint is based on the morphology and major element distribution within melilite, and is firm.

SHOCK CODE

Inputs

Our computation of the evolution of the gas and solids encountering a shock is restricted to a range of distances x from the shock front. Our computational domain extends a distance $x = -X_{pre}$ in the pre-shock region, to $x = 0$ at the shock front, to $x = +X_{post}$ in the post-shock region. The lateral extent of the shock front is assumed to greatly exceed either of these two values, so that a one-dimensional calculation will suffice. We typically use $X_{pre} \approx X_{post} \approx 10^5$ km, which are much smaller than the scale height of the nebula at 2–3 AU (approximately a few $\times 10^7$ km), so that a one-dimensional calculation is applicable to nebula shocks generated by diskwide gravitational instability (but not to bow shocks of planetesimals). Our computational domain is divided into 1000 zones.

The gas is divided into four populations: atomic hydrogen (H), molecular hydrogen (H_2), helium atoms (He), and molecules resulting from the evaporation of solids, which we represent with SiO. The ratio of heat capacities, γ, is defined as 5/3 for the two atomic species, and 7/5 for the two molecular species. There is a chemical energy of 4.48 eV associated with the dissociation of each H_2 molecule. Solids are divided into J populations of identical particles, indexed by j. Unique to each population are the number density n_j of particles, their velocity V_j, their temperature T_j, and their radii a_j. Also defined for each population are: the material density ρ_j; the heat capacity $C_{P,j}$; the latent heat of fusion $l_{melt,j}$ and the temperature range ΔT_j over which melting takes place (between the solidus and liquidus temperatures); and the latent heat of evaporation $l_{evap,j}$ and the temperature $T_{evap,j}$ at which evaporation proceeds. Melting effectively increases the heat capacity over the range of temperatures over which melting occurs, by an amount $l_{melt,j}/\Delta T_j$. We assume identical material chacteristics for all of the populations $C_P = 1.0 \times 10^7$ erg g^{-1} K^{-1}, $l_{melt} = 5.0 \times 10^9$ erg g^{-1}, and $l_{evap} = 1.1 \times 10^{11}$ erg g^{-1}, and $T_{evap} = 2000$ K (Wasson, 1996). Melting is assumed to take place between temperatures of 1400 and 1820 K, so that $\Delta T = 420$ K. Over this temperature range, the heat capacity is effectively 2.19×10^7 K. The fraction of the chondrule melted is 0% at 1400 K, and rises linearly to 100% at 1820 K. A final needed parameter for each solids population is the radiative emissivity ε_j. Since the chondrules are heated to temperatures 1500–2000 K, the wavelength of peak thermal emission is by Wien's law ~2 μm. The Planck-averaged emissivity ε is proportional to the particle radius a for small silicate particles, but independent of size for large particles (Draine and Lee, 1984). We adopt the following emissivity, to conform with the results of Draine and Lee (1984):

$$\varepsilon_j = 0.8 \times \min\left[1, \left(\frac{a_j}{2\ \mu\text{m}}\right)\right] \quad (3)$$

We adopt the same wavelength-averaged emissivity for absorption and emission since both absorbed and emitted spectra are in the same wavelength regime (the near infrared).

Finally, we also include the effects of dust, fine-grained silicate particles that are well-coupled to the gas. Because of the small sizes (<1 μm) of dust grains, they have exceedingly low masses and thermal inertias. As such, their thermal and aerodynamic timescales are too small to allow the (explicit) numerical code to follow their evolution as it does the larger, chondrule-sized particles. We therefore assume that all dust particles are dynamically well coupled to the gas, and are always in thermal equilibrium with the gas and the radiation field. Using an emissivity $\varepsilon = 0.2$, we calculate the temperature of the dust particles using Eq. (14), but with that equation's left-hand side set to zero. The assumption of good dynamical coupling between gas and dust underestimates the temperature reached by dust since it neglects the frictional drag heating of dust. If the equilibrium temperature is >2000 K, then we assume that dust is destroyed, and its mass added to the gas, from that point until the end of the post-shock region. The presence or absence of dust is used to set the opacity of the gas in that region so that the radiation field can be calculated properly.

Radiative Transfer

Solids are allowed to absorb and emit radiation, which affects their energy budget. The radiation some particles emit may be absorbed by other particles at a distant location. The determination of the radiation field at all locations is therefore a nontrivial but crucial calculation. The gas itself may also radiate, primarily due to vibrational modes of H_2O near 6 μm (Neufeld and Kaufman, 1993). Treatment of the especially difficult problem of line radiation in a dusty medium has been discussed in Hollenbach and McKee (1979). Following the formulation of Neufeld and Kaufman (1993), we estimate that the shock region will be too optically thick to its own line emission to lose more than ~10% of its energy. At any rate, we neglect cooling of the gas due to line emission in our treatment of the radiation field. We follow the approach outlined in Mihalas (1978), for the radiation emergent from plane-parallel, temperature-stratified slab atmospheres.

The first parameter to be defined is the optical depth (distance in units of the mean free path of photons) at all locations. At the post-shock boundary, the optical depth $\tau(x = +X_{\rm post}) \equiv 0$, increasing to a maximum value $\tau(x = -X_{\rm pre}) \equiv \tau_{\rm m}$ at the pre-shock boundary. At other locations,

$$\tau(x) = \int_{x'=x}^{x=+X_{\rm post}} \left(\rho_{\rm g}\kappa + \sum_{j=1}^{J} n_j \pi a_j^{\,2} \varepsilon_j\right) {\rm d}x' \qquad (4)$$

where $\kappa \approx 1.14$ cm^2 g^{-1} is the opacity of the gas, with density $\rho_{\rm g}$, due to dust associated with it. This value of κ is chosen to correspond to silicate dust particles totalling 0.125% of the mass of gas, and is consistent with (although slightly lower than) estimates of the opacity in protoplanetary disks (Draine and Lee, 1984; Ossenkopf and Henning, 1994; Henning and Stognienko, 1996). If at some point the gas is so hot and dense that dust is destroyed (see the previous section), then κ is set to zero from that point on.

The second parameter to be defined is the source function, S. The source function from a blackbody at temperature T is the Planck function $B(T)$, which after integrating over wavelength is $B(T) = \sigma T^4$, where σ is the Stefan–Boltzmann constant (our radiative terms S, B and J are a factor of π greater than their usual definitions, for ease of notation). If all the particles in a region are held at temperature T, the source function must approach B, regardless of the emissivities of the particles. If the particles are at different temperatures, the source function is weighted according to their emissivities:

$$S = \frac{\rho_{\rm g}\kappa\sigma T_{\rm g}^{\,4} + \sum_{j=1}^{J} n_j \pi a_j^{\,2} \varepsilon_j \sigma T_j^{\,4}}{\rho_{\rm g}\kappa + \sum_{j=1}^{J} n_j \pi a_j^{\,2} \varepsilon_j} \qquad (5)$$

This reduces to $\sigma T_{\rm g}^4$ in the event that all $T_j = T_{\rm g}$ are identical. (Although the temperature of dust is approximated in the code, the gas temperature is used for the source function from dust to avoid numerical instabilities, and because the two are so similar.) The last parameter to be specified is the radiation entering through the two computational boundaries (integrated over wavelength). The radiation field entering the pre-shock computational boundary is given by $I_{\rm pre} = \sigma T_0^4$, where T_0 is the temperature of the ambient medium. The radiation field entering the post-shock boundary is given by $I_{\rm post} = \sigma T_{\rm jump}^4$, where $T_{\rm jump}$ is the post-shock equilibrium temperature, using the radiative jump conditions of "Jump Conditions". This treatment assumes that over the course of chondrule formation (a few days at most), the post-shock gas cannot cool by radiation to a cooler, unshocked region. This is consistent with nebular shocks from diskwide gravitational instability, since by Eq. (2), for typical nebula parameters the cooling time is longer than days.

Given the incident radiation fields and the source function at all optical depths, $S(\tau)$, the mean intensity of radiation, $J(\tau)$ (integrated over wavelength) can be found:

$$J(\tau) = \frac{I_{\rm pre}}{2} {\rm E}_2(\tau_{\rm m} - \tau) + \frac{I_{\rm post}}{2} {\rm E}_2(\tau) + \frac{1}{2} \int_0^{\tau_{\rm m}} S(t) {\rm E}_1 |t - \tau| {\rm d}t \qquad (6)$$

where $\rm E_1$ and $\rm E_2$ are exponential integrals. Using the properties of the exponential integrals, namely that ${\rm dE}_n(x)/{\rm d}x = -{\rm E}_{n-1}(x)$, it can be shown by direct integration that if $S(t) = I_{\rm pre} = I_{\rm post} = I_0$ everywhere, then $J(\tau) = I_0$. We can also solve for the net flux of radiation energy, $F_{\rm rad}(\tau)$:

$$F_{\rm rad}(\tau) = +2I_{\rm pre}\mathrm{E}_3(\tau_{\rm m}-\tau) + 2\int_{\tau}^{\tau_{\rm m}} S(t)\mathrm{E}_2(t-\tau)\mathrm{d}t - 2I_{\rm post}\mathrm{E}_3(\tau) - 2\int_0^{\tau} S(t)\mathrm{E}_2(\tau-t)\mathrm{d}t \quad (7)$$

It is again possible to show by direct integration that in the case $S(t) = I_{\rm pre} = I_{\rm post} = I_0$ everywhere that the net flux $F_{\rm rad} = 0$. It is also straightforward to demonstrate that in general

$$\frac{\partial F_{\rm rad}}{\partial x} = -4\rho_{\rm g}\kappa\left[J_r - \sigma T_{\rm g}{}^4\right] - \sum_{j=1}^{J} n_j\, 4\pi a_j{}^2 \varepsilon_j \left[J_r - \sigma T_j{}^4\right] \quad (8)$$

where κ is the opacity of the gas (*via* the well-coupled dust component).

Dynamics and Energetics

It is best to begin a discussion of the dynamics and energetics from the viewpoint of the particles. Since we assume that particles are not destroyed (evaporation only shrinks them in radius to a minimum size), the continuity equation for each population j of particles holds:

$$\frac{\partial}{\partial x}(n_j V_j) = 0 \quad (9)$$

The force equation on the particles is given by

$$n_j m_j V_j \frac{\partial V_j}{\partial x} = n_j F_{{\rm drag},j} \quad (10)$$

where m_j is the mass of the particles of population j (which may change due to evaporation), and the drag force on each particle is given by

$$F_{{\rm drag},j} = -\pi a_j{}^2 \left(\frac{C_{{\rm D},j}}{2}\right)\left|V_j - V_{\rm g}\right|\left(V_j - V_{\rm g}\right) \quad (11)$$

(Probstein, 1968; Gombosi *et al.*, 1986). The drag coefficient $C_{{\rm D},j}$ is found according to formulas in Gombosi *et al.* (1986), and is given in appendix A. If $V_j > V_{\rm g}$, then Eq. (11) shows that the force on the particles is in the negative direction, slowing them down, while if $V_j < V_{\rm g}$, then the force is in the positive direction, speeding them up.

The frictional drag can heat particles; particles can also absorb or give up thermal energy to the gas. The net rate at which the thermal energy of a particle increases is $4\pi a_j{}^2 q_j$ per particle, where

$$q_j = \rho_{\rm g} C_{{\rm H},j}(T_{\rm rec} - T_j) \quad (12)$$

Expressions for $C_{{\rm H},j}$, the heat transfer coefficient, and $T_{\rm rec}$, the "recovery temperature", which depend on the gas properties and relative velocity of the solids and gas, are taken from Gombosi *et al.* (1986) and presented in appendix A. In practice, we treat the four gas species separately, then combine their separate heating rates into one overall heating rate. The net heating rate per unit area is then the q_j plus the radiative terms: $q_j + \epsilon_j(J_r - \sigma T_j{}^4)$. This net heating rate goes into raising the particle's temperature, melting it, or causing it to evaporate. If $T_j < T_{{\rm evap},j}$, or if $T_j = T_{{\rm evap},j}$ and the net heating is negative, then there is no evaporation, m_j is constant, and

$$\frac{\partial a_j}{\partial x} = 0 \quad (13)$$

$$\frac{\partial}{\partial x}\left(C_{{\rm P},j} T_j\right) = \frac{3}{\rho_j a_j V_j}\left[q_j + \varepsilon_j (J_r - \sigma T_j{}^4)\right] \quad (14)$$

If $T_j \geq T_{{\rm evap},j}$ and the net heating is positive, then all the heat goes into evaporating the particle:

$$\frac{\partial a_j}{\partial x} = -\frac{1}{\rho_j l_{{\rm evap},j} V_j}\left[q_j + \varepsilon_j (J_r - \sigma T_j{}^4)\right] \quad (15)$$

and

$$\frac{\partial T_j}{\partial x} = 0 \quad (16)$$

(That is, T_j is held constant at $T_{{\rm evap},j}$.) The above $4 \times J$ equations can be used to immediately solve for the $4 \times J$ solids unknowns, n_j, V_j, a_j and T_j.

The gas equations are as follows. Hydrogen atoms and molecules obey the following continuity equations:

$$\frac{\partial}{\partial x}(n_{\rm H} V_{\rm g}) = -2R \quad (17)$$

and

$$\frac{\partial}{\partial x}(n_{\rm H_2} V_{\rm g}) = +R \quad (18)$$

where R is the net rate (per unit volume and unit time) of the reactions $\mathrm{H} + \mathrm{H} \rightarrow \mathrm{H_2}$, given in appendix B. The total number of hydrogen nuclei are conserved. Helium atoms are neither created or destroyed:

$$\frac{\partial}{\partial x}(n_{\rm He} V_{\rm g}) = 0 \quad (19)$$

The other molecules formed by the evaporation of solids are created at a rate

$$\frac{\partial}{\partial x}(n_{\rm SiO}V_{\rm g}) = -\sum_{j=1}^{J}\frac{n_j V_j\, 4\pi\rho_j\, a_j{}^2}{44m_{\rm H}}\frac{\partial a_j}{\partial x} \equiv \dot{N}_{\rm SiO} \qquad (20)$$

Because the gas species are assumed to be dynamically and thermally well coupled and to share the same velocity and temperature, we need write just one force equation for the gas. Defining $C_{\rm s}{}^2 \equiv kT_{\rm g}/m_{\rm H}$,

$$\frac{\partial}{\partial x}\Big((n_{\rm H}+2n_{\rm H_2}+4n_{\rm He}+44n_{\rm SiO})V_{\rm g}{}^2 + (n_{\rm H}+n_{\rm H_2}+n_{\rm He}+n_{\rm SiO})C_{\rm s}{}^2\Big) = -\frac{1}{m_{\rm H}}\sum_{j=1}^{J} n_j\left[F_{{\rm drag},j} + 4\pi a_j{}^2\rho_j V_j{}^2\frac{\partial a_j}{\partial x}\right] \qquad (21)$$

The last term accounts for the momentum flux lost from the particles as they evaporate and lose mass; the evaporated mass becomes part of the gas and transfers momentum to it.

All that is lacking to specify the evolution of the gas is an energy equation. Like the solids, the gas can be heated by frictional drag as well as by collisional transfers of thermal energy. Because the total energy must be conserved, it is best to begin with a combined energy equation for the solids and gas. All stores of energy are moving with the gas or particles, except for the radiation:

$$\frac{\partial}{\partial x}\left[(n_{\rm H}V_{\rm g}\left(\frac{1}{2}m_{\rm H}V_{\rm g}{}^2+\frac{5}{2}kT_{\rm g}\right)+n_{\rm H}V_{\rm g}e_{\rm diss}+ n_{\rm H_2}V_{\rm g}\left(\frac{1}{2}2m_{\rm H}V_{\rm g}{}^2+\frac{7}{2}kT_{\rm g}\right)+n_{\rm He}V_{\rm g}\left(\frac{1}{2}4m_{\rm H}V_{\rm g}{}^2+\frac{5}{2}kT_{\rm g}\right)+ n_{\rm SiO}V_g\left(\frac{1}{2}44m_{\rm H}V_{\rm g}{}^2+\frac{7}{2}kT_{\rm g}\right)+ \sum_{j=1}^{J} n_j m_j V_j\left(\frac{1}{2}V_j{}^2+C_{{\rm P},j}T_j\right)\right] = -\frac{\partial F_{\rm rad}}{\partial x} = +4\rho_{\rm g}\kappa(J_r-\sigma T_{\rm g}{}^4)+\sum_{j=1}^{J} n_j\,4\pi a_j{}^2\varepsilon_j\,(J_r-\sigma T_j{}^4) \qquad (22)$$

where $e_{\rm diss} = 2.24$ eV. After subtracting the terms in the dust energy evolution, and simplifying using the continuity equations, all the radiative terms involving particle opacities drop out, as they should, and only the gas opacity is relevant to the heating of the gas. What remains is

$$(n_{\rm H}+n_{\rm H_2}+n_{\rm He}+n_{\rm SiO})V_{\rm g}{}^2\left(\frac{\partial V_{\rm g}}{\partial x}\right)+ \left(\frac{5}{2}n_{\rm H}+\frac{7}{2}n_{\rm H_2}+\frac{5}{2}n_{\rm He}+\frac{7}{2}n_{\rm SiO}\right)V_{\rm g}\left(\frac{\partial C_{\rm s}{}^2}{\partial x}\right)= +\frac{4\rho_{\rm g}\kappa}{m_{\rm H}}(J_r-\sigma T_{\rm g}{}^4)-\sum_{j=1}^{J} n_j\,4\pi a_j{}^2\frac{q_j}{m_{\rm H}}- \sum_{j=1}^{J} n_j V_j\frac{F_{{\rm drag},j}}{m_{\rm H}}-\sum_{j=1}^{J} n_j V_j\left(\frac{4\pi a_j{}^2\rho_j}{m_{\rm H}}\frac{\partial a_j}{\partial x}\right)\times \left(\frac{1}{2}V_j{}^2-\frac{1}{2}V_{\rm g}{}^2\right)+R\left(\frac{3}{2}C_{\rm s}{}^2-\frac{2e_{\rm diss}}{m_{\rm H}}\right)-\dot{N}_{\rm SiO}\left(\frac{7}{2}C_{\rm s}{}^2\right) \qquad (23)$$

The first term on the right-hand side of Eq. (23) accounts for energy absorbed by the gas from the radiation field, and radiation emitted by the gas (through the well-coupled dust component). The second term accounts for the loss of thermal energy from the gas to the particles. The third term includes work done by the gas on the particles *via* the drag acceleration. The fourth term accounts for changes in the gas kinetic energy due to the creation of new gas molecules by evaporation. The fifth term accounts for changes in the thermal and chemical energy due to dissociations and recombinations. Finally, the sixth term accounts for changes in the thermal energy due to the addition of new molecules by evaporation of solids. Likewise, the force equation can be rewritten, as

$$\Big[(n_{\rm H}+2n_{\rm H_2}+4n_{\rm He}+44n_{\rm SiO})V_{\rm g}{}^2 - (n_{\rm H}+n_{\rm H_2}+n_{\rm He}+n_{\rm SiO})C^2\Big]\left(\frac{\partial V_{\rm g}}{\partial x}\right)+ V_{\rm g}(n_{\rm H}+n_{\rm H_2}+n_{\rm He}+n_{\rm SiO})\left(\frac{\partial C_{\rm s}{}^2}{\partial x}\right)= \frac{V_{\rm g}}{m_{\rm H}}\sum_{j=1}^{J} n_j\left[-F_{{\rm drag},j}+4\pi a_j{}^2\rho_j V_j{}^2\frac{\partial a_j}{\partial x}\right]+ RC_{\rm s}{}^2-\dot{N}_{\rm SiO}\left(44V_{\rm g}{}^2+C_{\rm s}{}^2\right) \qquad (24)$$

To solve the above equations, the particles and gas are started at the pre-shock computational boundary with imposed initial conditions. They both begin with the same arbitrary temperature T_0 and velocity V_s. There is initially no SiO vapor or atomic H. The number density of He atoms is 0.2× the density of H_2 molecules. The equations are numerically integrated using a fourth-order Runge–Kutta scheme with variable step

sizes. The integration proceeds from one grid zone boundary to the next; the variable step sizes refer to the steps needed to integrate across each grid zone. Integration relies on specifying the spatial derivatives of each variable. This is easily accomplished by solving for each derivative in the proper order. First the particles' radii, temperatures and velocities are found directly from Eqs. (10) and (13–16). From the continuity Eq. (9), the particle densities are found. Next, Eqs. (23) and (24) are combined to solve for the two unknowns V_g and T_g. Substituting the derivative of V_g allows us to find the derivatives of all the gas densities, thereby closing the system of equations. One exception is at the shock front, where the jump conditions (see the next section) mandate a near-instantaneous change in the gas properties. Particle properties are not changed across the shock front. Also, if the relative velocity between gas and particles drops under 1 m s^{-1} in the post-shock region, the relative velocity is set to zero, and the particles are forced to move with the gas from that point on. The numerical integration has an internal accuracy of 10^{-6}.

During the integrations, the radiation field is considered fixed. Initially, it is assumed that $J = \sigma T_0^4$ in the pre-shock region, and $J = \sigma T_{\rm jump}^4$ ("Jump Conditions") in the post-shock region. After all other variables have been integrated across the entire computational domain, however, the radiation field is recalculated based on the updated particle densities, radii and temperatures. The particles and gas are sent through the shock again, their temperatures calculated based on the new radiation field. The solution is iterated until the radiation field and the particle temperatures are self-consistent. In the standard run, convergence of particle temperatures everywhere to within 1 K and convergence in J_r to within 0.1% were achieved in ~150 iterations.

Jump Conditions

Two sets of jump conditions are used to quantify the change in gas properties in two regimes: directly across the shock front; and very far away from the shock front, after the gas and solids have reached equilibrium. The first set of jump conditions is needed to calculate the increase in gas temperature, pressure and density immediately behind the shock. The second set of jump conditions is needed to calculate the final, common temperature of gas and solids. This temperature is used to define the radiation boundary condition in the post-shock region.

The shock front is the viscous layer in which the gas motions change from supersonic to subsonic and kinetic energy is converted into heat. It is only a few gas mean-free paths thick. The cross section of an H_2 molecule is $\sim 5 \times 10^{-16}$ cm^2, so that for typical densities $n_{H_2} \approx 10^{14}$ cm^{-3}, the shock front is only meters thick. Gas and particles will pass through this layer in ~100 μs. By integrating Eq. (22) across the shock front, starting only a few meters ahead and ending a few meters behind the shock, there is no time for many of the terms in Eq. (22) to change appreciably. The dissociation of hydrogen takes $\gtrsim$1 s, and no evaporation occurs in the first several seconds, either. Likewise, the optical depth across 10 m of dust and chondrules will not exceed one part in 10^5; thus, the flux $F_{\rm rad}$ just ahead of the shock front will be virtually identical to the flux behind it. Since the energy density of radiation ($\sim \sigma T^4/c \approx 0.03$ erg cm^{-3}) is already a small fraction of the material energy density ($\sim nkT \approx 30$ erg cm^{-3}), a 10^{-5} variation in it will have negligible effect on the gas over only 10 m. Finally, the particles are unable to heat up appreciably in less than a millisecond, and neither do their velocities vary on timescales less than ~10 s. In summary, we need only consider the species H, H_2 and He, and while their densities will increase behind the shock, the proportions of these three species do not change. Thus we can use the usual jump conditions (*e.g.*, Shore, 1992):

$$\rho_2 = \rho_1 \frac{(\gamma+1)\mathrm{M}^2}{(\gamma-1)\mathrm{M}^2+2} \tag{25}$$

$$V_2 = V_1 \frac{n_1}{n_2} \tag{26}$$

$$T_2 = T_1 \frac{[2\gamma\,\mathrm{M}^2-(\gamma-1)][(\gamma-1)\mathrm{M}^2+2]}{(\gamma+1)^2\mathrm{M}^2} \tag{27}$$

where

$$\mathrm{M}^2 = \left[\frac{n_{\rm H}+2n_{\rm H_2}+4n_{\rm He}}{n_{\rm H}+n_{\rm H_2}+n_{\rm He}}\right]\frac{m_{\rm H}V_1^{\,2}}{kT_1} \tag{28}$$

is the square of the Mach number, subscript 1 denotes pre-shock conditions, and subscript 2 post-shock conditions. To accomodate to the multiple species of the gas, one need only interpret the ratio of specific heats, γ, correctly:

$$\gamma = \frac{\frac{5}{2}n_{\rm H}+\frac{7}{2}n_{\rm H_2}+\frac{5}{2}n_{\rm He}}{\frac{3}{2}n_{\rm H}+\frac{5}{2}n_{\rm H_2}+\frac{3}{2}n_{\rm He}} \tag{29}$$

For a solar composition gas at ~300 K, $n_{\rm H} \approx 0$, and $n_{\rm He}/n_{\rm H2} \approx 0.2$, so $\gamma \approx 1.429$. Immediately behind a very strong shock, the gas should be compressed by a factor of 5.67. Behind our canonical shock with $V_s = 7$ km s^{-1}, $\rho_1 = 10^{-9}$ g cm^{-3} and $T_1 = 300$ K, the density increases by a factor of 5.14, and the temperature increases by a factor of 10.51.

Very far away from the shock front, many optical depths ($\gtrsim 10^5$ km) away, one must use a different set of jump conditions, to derive the final temperature of the gas and solids. The gas can be assumed to be optically thick, and the solids and gas all in thermal and radiative equilibrium with a common

temperature. The gas and particles can also be considered to be in dynamical equilibrium. Under these conditions, one can apply the jump conditions of Hood and Horanyi (1993):

$$\rho_1 V_1 = \rho_2 V_2 \tag{30}$$

$$\frac{\rho_1 k T_1}{m} + \rho_1 V_1^{\,2} = \frac{\rho_2 k T_2}{m} + \rho_2 V_2^{\,2} \tag{31}$$

$$\frac{\gamma}{\gamma-1}\frac{kT_1}{m} + \frac{1}{2}V_1^{\,2} + \frac{\sigma T_1^{\,4}}{\rho_1 V_1} = \frac{\gamma}{\gamma-1}\frac{kT_2}{m} + \frac{1}{2}V_2^{\,2} + \frac{\sigma T_2^{\,4}}{\rho_1 V_1} \tag{32}$$

From these, one must solve for the density and temperature jumps simultaneously:

$$\frac{\rho_2}{\rho_1} \equiv \xi = \mathrm{M}^2 \frac{\Gamma - 1}{\mathrm{M}^2 + \Gamma} \tag{33}$$

and

$$\frac{T_2}{T_1} \equiv \zeta = 1 - \left(\frac{\xi - 1}{\xi^2}\right)\left(\xi - \mathrm{M}^2\right) \tag{34}$$

where

$$\Gamma \equiv \frac{2\gamma}{\gamma - 1} + \left(\frac{2m\sigma T_1^{\,3}}{\rho_1 V_1 k}\right)\left(\frac{\zeta^4 - 1}{\zeta - 1}\right) \tag{35}$$

For our nominal case with $V_s = 7$ km s^{-1}, $\rho_1 = 10^{-9}$ g cm^{-3} and $T_1 = 300$ K, $\mathrm{M}^2 = 46.1$, $\Gamma = 16.2$, $\xi = 11.2$, and $\zeta = 3.81$. Very far from the shock front, the final gas temperature is 1143 K (as opposed to 3153 K directly behind the shock front), and is compressed to densities twice as great as those immediately behind the shock front. This final temperature, denoted here as $T_{\mathrm{jump}} = \zeta T_0$, is the common temperature of gas and solids far from the shock front in the post-shock region. The radiation coming from these far reaches of the post-shock region must therefore be blackbody radiation at the temperature T_{jump}. This provides the needed boundary condition on calculation of J_r. It is also worth noting that if T_{jump} were to exceed the solidus temperature, then chondrules would reach an equilibrium in which they would not completely resolidify, and therefore could not be said to crystallize over the course of hours. As this is inconsistent with chondrules' textural evidence, we reject cases where $T_{\mathrm{jump}} \gtrsim 1400$ K. In the example just given above, the minimum temperature was 1143 K, but if the same shock were to propagate through a gas with $\rho_1 = 10^{-8}$ g cm^{-3}, the minimum temperature would be 1696 K. As such, we can rule out such high densities *a priori*.

RESULTS

Canonical Shock

Using the numerical code of the previous section, we have calculated the thermal histories of chondrules overrun by nebular shocks. Although the code is capable of including more than just the dust component in the gas and the single size of chondrule precursor we consider here, we defer an inclusion of multiple particle sizes to a future paper. The chondrule precursors are here assumed to be spherical, with radius 300 μm, and density 3.3 g cm^{-3}. It is assumed that averaged over the nebula, the mass of solids is a fraction 0.005 of the mass of gas, and that, consistent with the proportions in ordinary chondrites, 75% of the solids' mass is in the form of chondrule precursors. The fraction of the gas mass that is chondrules is therefore 0.00375 when averaged over the nebula. The actual density of chondrules overrun by the shock is increased or decreased by a concentration factor C relative to this fraction, and several cases of C are studied. The gas density and temperature are chosen to correspond to theoretical models of protoplanetary disks during their early, gravitationally unstable stages. We assume the model of Bell *et al.* (1997), using input values of angular momentum transport coefficient $\alpha = 10^{-4}$, and mass accretion rate $\dot{M} = 1 \times 10^{-8}$ M$_\odot$ year^{-1}, the median mass accretion rate among 1 Ma old T Tauri stars (Hartmann *et al.*, 1998). Such disks happen to be gravitationally unstable beyond 5 AU but stable inward of that radius. The density and temperature at the midplane at 2.5 AU in the Bell *et al.* model with these inputs are on the order of 1×10^{-9} g cm^{-3} and 300 K. The assumed shock velocity, 7 km s^{-1}, is about a third of the orbital velocity at 2.5 AU. In "Discussion, Pre-Shock Heating" we show that shock speeds of this order are consistent with shocks generated by gravitational instability.

For the canonical run described above ($C = 1$), the variation of gas velocity, density, temperature and pressure as a function of distance z from the shock front are displayed in Fig. 1. In the pre-shock region, the gas properties remain constant until within ~10^5 km of the shock front. There the co-moving chondrules absorb radiation from the other side of the shock front. The hot chondrules transfer heat to the gas by thermal collisions, and the gas temperature and pressure increase. The increase in pressure exerts a backward force on the gas, and its velocity decreases and its density increases. Before the gas even reaches the shock front, its velocity has slowed from 7 to 6.15 km s^{-1}, and its temperature has increased from 300 to 1736 K. The decrease in velocity and the increase in the sound speed reduce the Mach number from 6.78 to only 2.48. If radiation was more effective, the diffusion of energy across the shock front would change the shock into a subsonic flow with no sharp boundary. In the shock considered here, the flow remains supersonic, and the change in state of the gas is abrupt, although the impact across the shock front is lessened. Despite this, the post-shock temperature is not

much affected by the radiation diffusion, and is 3120 K right after the shock hits.

Soon after the shock hits, the hydrogen in the gas finds itself out of equilibrium at such a high temperature. Dissociation of hydrogen is rapid, and each dissociation consumes 4.48 eV per hydrogen molecule. Figure 2 shows the number densities of atomic and molecular hydrogen, and helium, during the minute before and after the shock hits. The gas cools rapidly from 3120 K, reaching temperatures ~2400 K in ~1.6 s, and 2000 K after 13 s. At that point, the mix of atomic and molecular hydrogen (which reaches equilibrium very quickly) has 6.1% of all hydrogen nuclei in atomic form. We allow for the dust grains to evaporate, but they do not do so in the canonical run.

The radiation field J_r is plotted in Fig. 3, given as an effective temperature $T_{\rm rad}$ ($J_r \equiv \sigma T_{\rm rad}^4$), along with the chondrule temperature $T_{\rm c}$. The differences between the two temperatures are small, showing that the chondrules are usually close to radiative equilibrium. Where $T_{\rm rad} > T_{\rm c}$ the net effect of the chondrule's interaction with the radiation field is to absorb radiation and be heated, while the chondrule experiences net cooling when $T_{\rm c} > T_{\rm rad}$. Chondrules in the post-shock region within ~100 km of the shock front experience a net cooling,

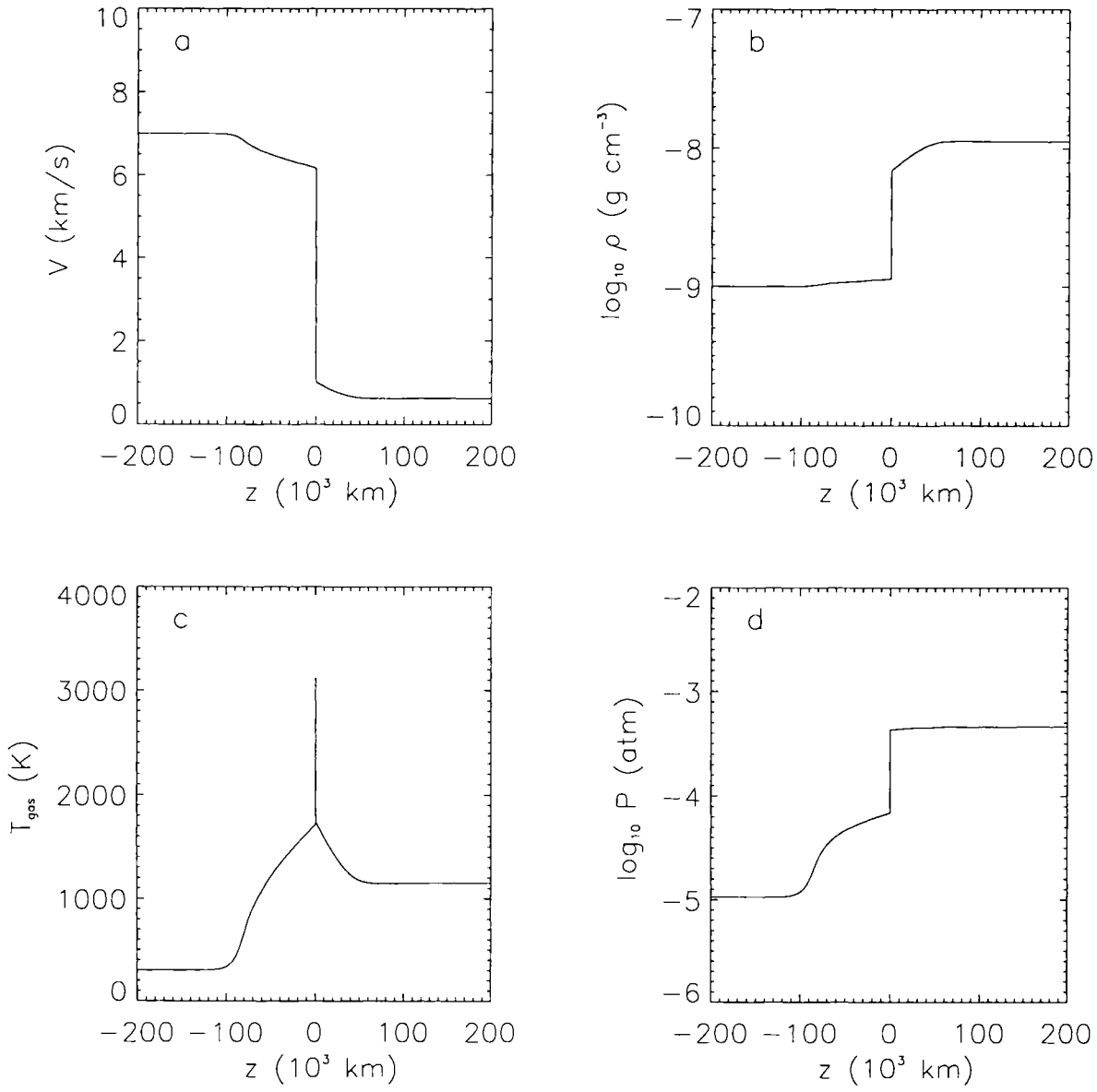

FIG. 1. Gas properties as a function of the distance z from the shock front. The pre-shock region here and in Fig. 3 is on the left. A steady state is assumed; the properties of an individual gas parcel as a function of time are found by reading these graphs from left to right. The gas velocity (a) decreases from 7 to 6.2 km/s as the shock front is approached, and the density (b) increases, because the increase in gas temperature (c) within 10^5 km of the shock front increases the gas pressure (d). The heating of the gas in the pre-shock region is due to thermal exchange with irradiated chondrules. The spike in the temperature at the shock front occurs immediately after passage of the shock, but before H_2 can dissociate. As the gas cools, pressure and density increase in the post-shock region.

but only $\lesssim$50% of the cooling they would experience if they absorbed no radiation. The radiation they emit as they cool propagates away from the shock front and heats chondrules in other regions. The post-shock chondrules within ~10 optical depths of the shock front (~7×10^4 km) experience a net heating, as do chondrules that have not even yet reached the shock front. About 10 optical depths (one optical depth = 8×10^3 km in pre-shock gas) before chondrules reach the shock front, they begin to heat up, an inevitable consequence of the fact that radiation travels faster than even a shock wave.

The thermal history of the chondrule, including heating and cooling from interactions with the gas and radiation fields, is illustrated in Fig. 4. The sequence of events is as follows. At very long times before the chondrules reach the shock front, they are in equilibrium with the gas, staying at an ambient temperature here assumed to be 300 K. Beginning ~4 h before the shock front overtakes the chondrules, they begin absorbing

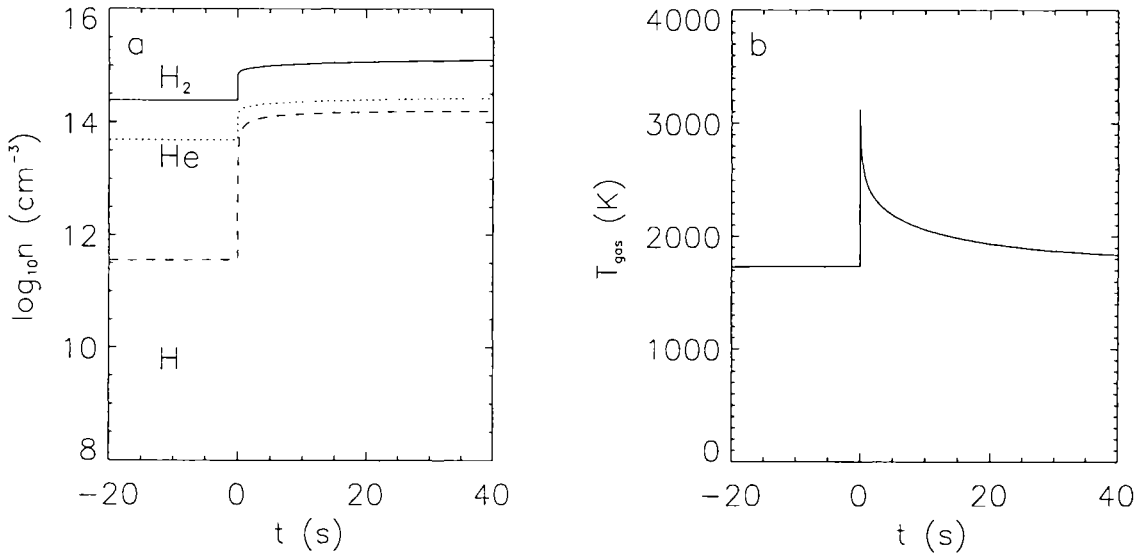

FIG. 2. Energetics of dissociation. (a) The number densities of molecular hydrogen (solid line), atomic hydrogen (dashed line) and helium atoms (dotted line) in the minute before and after shock passage. The cooling effect of hydrogen dissociation on the gas temperature is seen in (b).

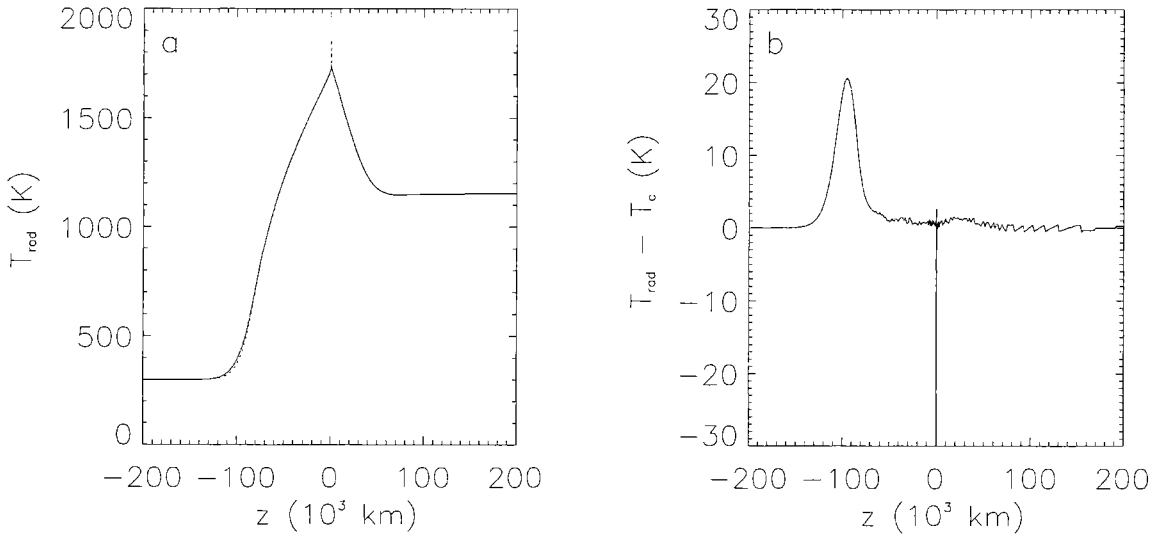

FIG. 3. Energetics of radiation. (a) Radiation field J_ν expressed as a radiation temperature T_{rad} (solid line), compared to chondrule temperature (dotted lines). The two are nearly equal, showing that chondrules reach radiative equilibrium. (b) The temperature differential, showing that chondrules are heated significantly by the radiation field at $z \approx -9 \times 10^4$ km from the shock front, whereas chondrules at the shock front emit more radiation than they absorb.

thermal radiation emitted by the chondrules that have already been through the shock front. This heats them up to 500 K 230 min before they pass through the shock front, 1000 K 170 min before the shock, and 1500 K 64 min before the shock hits. By the time they reach the shock front proper, the chondrules have already reached temperatures ~1742 K. After they pass through the shock front, they find themselves moving supersonically with respect to the gas, and gas-drag frictional heating heats them to a peak temperature of 1858 K at 1.6 s after the shock hits. After this peak, the temperature drops rapidly (~3×10^4 K h^{-1}) to a "baseline" temperature of ~1730 K, where the heating is due to absorption of radiation emitted by dust, and to thermal exchange with the gas, but not gas-drag heating. Once this baseline temperature is reached, the rate of change of the temperature is determined not by the particle dynamics, but by how quickly the particle can escape the zone of intense thermal radiation and hot gas. Analytical estimates ("Discussion, Cooling Rates") lead to a cooling rate ~50 K h^{-1}, consistent with the calculated cooling rates, which are in the range 35–50 K h^{-1} over the temperature range 1400–1700 K at which significant crystallization will take place.

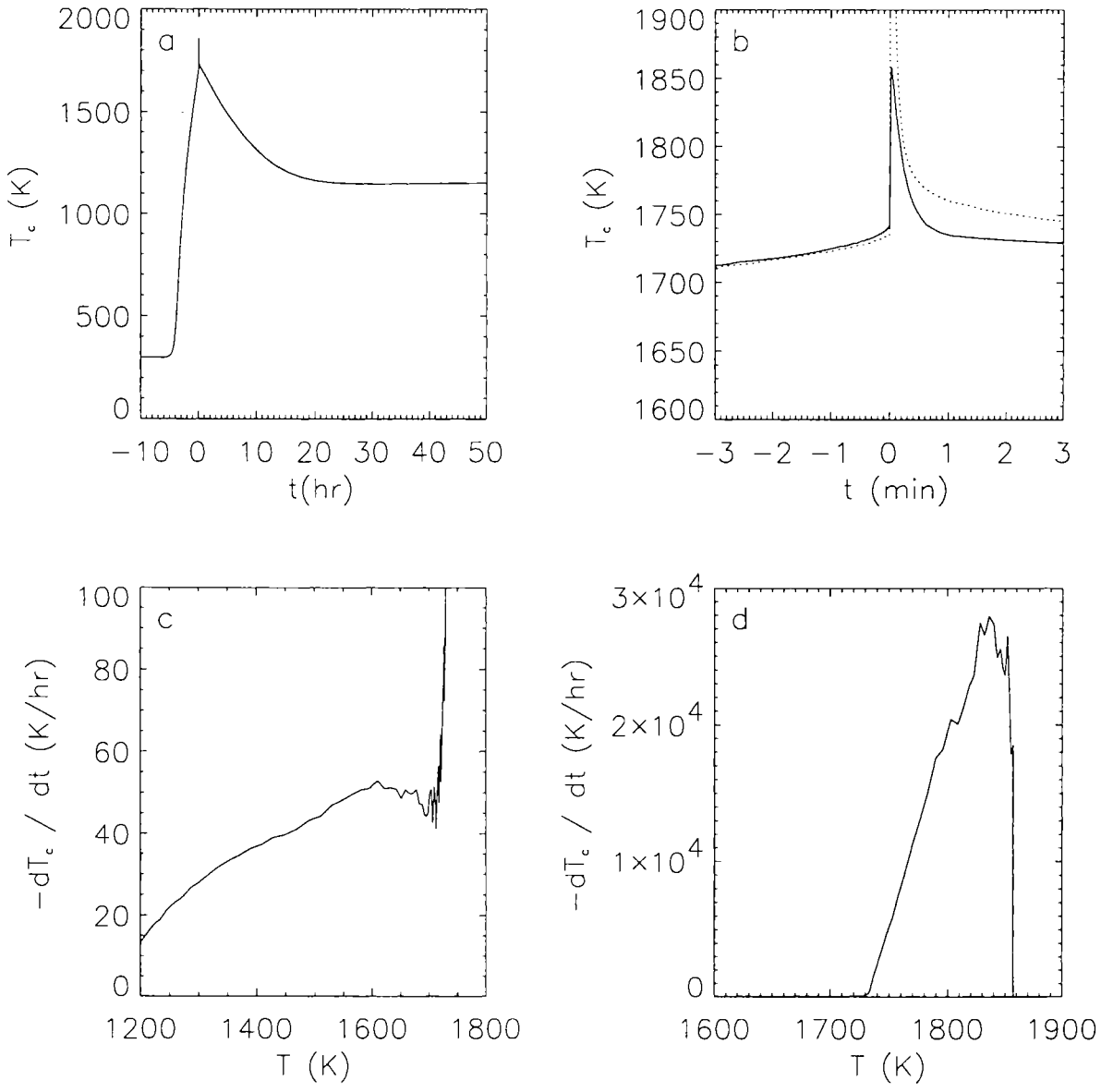

FIG. 4. Thermal history of chondrule in canonical shock. The chondrule's temperature (solid line) over the course of hours (a), and also minutes (b), where it is contrasted with the temperature of the gas (dotted line). Chondrules in the pre-shock region are heated by radiation, reaching 1000 K at 170 min before they reach the shock front. The cooling rates of the chondrules as a function of temperature are much slower through the crystallization temperatures 1400–1730 K (c) than at the higher temperatures 1730–1860 K (d), when heating is dominated by gas drag.

Effects of Radiation and Dissociation

Our next run considers the same canonical case as above, but with the important difference that J_r in Eq. (14) is set to a background value of $\sigma(300\ \mathrm{K})^4$. That is, particles may emit thermal radiation, but they do not absorb any radiation except that which would keep them at 300 K. This calculation represents the optically thin limit in which chondrules are (unrealistically) not allowed to absorb other chondrules' radiation, and is used to show that the slow cooling rates we obtain are *not* due to diffusion of radiation through an optically thick environment. The main effect of this change is to decrease the peak temperatures reached by the chondrules, from 1858 K to only 1388 K. In this sense, gas-drag heating alone heated the chondrule by ~1100 K, while radiation heated it an additional ~500 K. Likewise, the baseline temperature is much lower, being only ~950 K instead of ~1700 K. The thermal exchange of the gas can thus be thought of as raising the chondrule temperatures in the post-shock region by about 650 K, with radiation increasing these temperatures an additional 750 K. The interactions with the gas and with the radiation field have comparable effects on the chondrule temperatures. The cooling rates of the chondrules are not affected when they are not allowed to absorb the thermal emissions of other chondrules. After the gas-drag heating stage, the cooling rates are in the range 10–60 K h^{-1}. This indicates that the chondrule cooling rates are controlled by how quickly the gas can cool.

We also conducted a run identical to the canonical case except that hydrogen was not allowed to dissociate. Without this major sink of energy for the gas, the gas remained at 3160 K instead of cooling within minutes to ~1730 K, and the chondrule peak temperatures were consequently higher, being 1925 K instead of 1858 K.

Effect of Chondrule Density

We next consider the effect of changing the density of solids. This is motivated by the idea that chondrules may be selectively concentrated by turbulence (Cuzzi *et al.*, 1996, 2001). Defining C as the density of chondrules in some region normalized to the average density of chondrules everywhere, the average concentration over all volume is unity by definition. Turbulence can lead to $C >> 1$ in small regions, however—in a nebula with turbulence parameter $\alpha = 10^{-4}$, maximum concentrations of 10^6 can be achieved in small regions ~1 km in size (Cuzzi *et al.*, 1996). Such a zone has an optical thickness ~30 (assuming post-shock gas density 10^{-8} g cm^{-3}). The self-similarity of the turbulence tends to make constant the product of C and the size l of a region with concentration greater than C: $Cl \approx 10^6$ km (Desch and Cuzzi, 2000). This self-similarity implies that regions of any concentration C will all appear optically thick from the outside, and that regions of even higher concentration make up a negligible fraction of their volume. To a good degree of approximation, then, although zones of increased concentration are only limited in size and do not represent the nebula as a whole, our numerical code can be applied to these smaller regions as if C were uniform everywhere. Finally, we note that although the chondrule concentration averaged over all space is unity, a typical chondrule will experience a time-averaged concentration much greater than 1. Chondrules spend a significant fraction of their time in regions with $C > 100$ (Cuzzi *et al.*, 2001), and the average C experienced by chondrules is probably in the range 10–100 (J. Cuzzi, pers. comm.).

The effects of chondrule concentration on the peak temperatures and the cooling rates are displayed in Table 4. From Table 4, it is evident that the peak temperature reached by the chondrule is a strong function of the chondrule concentration, especially for $C \gtrsim 100$. This is due to our assumption that in the $C = 1$ case, chondrules make up 3.75×10^{-3} of the mass. The density of gas and solids combined in a $C = 100$ mixture is 40% higher than in the $C = 1$ case, while in the $C = 300$ mixture, it is over twice as high. Chondrules tend to drain the gas of thermal energy, due to their surface area, but they also heat the gas as the chondrules' kinetic energy is dissipated; there is a tendency for the gas to reach quasi-equilibrium temperatures that increase with C. More importantly, the absorption of the thermal radiation from nearby hot chondrules, which adds several hundred degrees Kelvin to the chondrules' temperatures in the $C = 1$ case, is even more important as C is increased. For the same gas density and shock speed, chondrules are heated to higher temperatures in zones with high concentrations. The effect on the cooling rate is more complicated, and depends on the temperature at which the cooling rate is sought, but cooling rates at 1600 K are $\lesssim$100 K h^{-1} for $C \lesssim 30$, and ~300 K, h^{-1} for $C \gtrsim 30$. The thermal history of a chondrule in a region with $C = 30$ is shown in Fig. 5, and the thermal history of a chondrule in a region with $C = 300$ is shown in Fig. 6. In the case with $C = 300$, ~10% of the chondrule mass has evaporated, elevating the oxygen fugacity by a factor of ~30. The trend for the peak temperature to increase with increasing concentration of chondrules reaches a limit: chondrules in regions with $C \gtrsim 500$ were found to evaporate completely. If ρ_{gas} and V_s are sufficient to evaporate particles in these high-C regions down to ~250 μm, then the evaporated silicate material will be comparable in mass

TABLE 4. Predicted cooling rates.

C	T_{peak} (K)	Cooling rate at 1600 K (K/h)	Dust evap.?
0.3	1856	50	N
1	1858	50	N
3	1860	50	N
10	1871	60	N
30	1887	85	N
100	1945	110	Y
300	>2000	400	Y
500	>2000	N/A	Y

to the mass of the gas. With the density of gas molecules nearly doubled, gas-drag heating was found to be even more efficient, leading to runaway evaporation of the chondrules.

Effects of Densities and Shock Speeds

The effects of gas density and shock speed are illustrated in Table 5, which shows the results of a parameter study in which ρ_{gas} could equal 3×10^{-10}, 1×10^{-9}, or 3×10^{-9} g cm^{-3}, and V_s could equal 5, 6, 7, 8, or 9 km s^{-1}. The peak temperatures and the cooling rate (through 1600 K) are displayed. If the peak temperature reached 2000 K, at which point the chondrule is assumed to evaporate, the final radius of the chondrule is also given. Also included is whether or not dust could be definitely said to evaporate for that run. As expected, chondrules will completely evaporate at high densities and/or high shock speeds, while chondrules at lower densities and/or shock speeds have peak temperatures $\lesssim$1400 K, meaning they were never melted and would not be recognized as chondrules today. (If chondrule precursors were fragile, fluffy aggregates, they might not survive such shocks at all.) The narrow band of parameter space that leads to chondrules, which were melted but not evaporated, also leads to roughly constant cooling rates in the range 10–100 K h^{-1} for these cases with $C = 1$. Higher chondrule concentrations are assumed to lead to more complete melting and faster cooling rates at all gas densities and shock speeds, as they did for the canonical case. Thus we can say with certainty that only porphyritic chondrules can form in

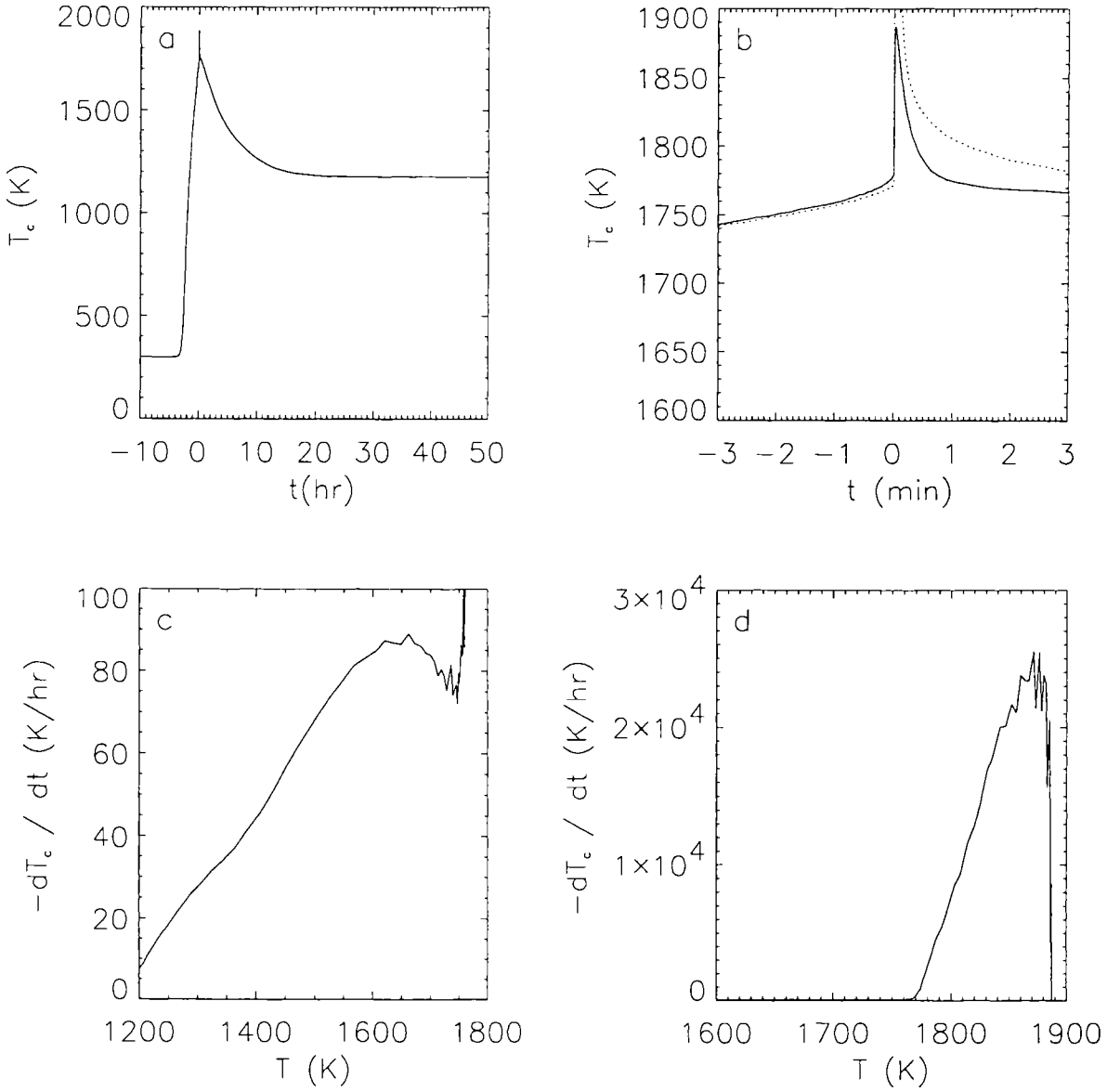

FIG. 5. Same as Fig. 4, but with chondrule concentration increased by a factor of 30 over the canonical "solar" value ($C = 30$). Peak temperatures and cooling rates are slightly higher than in the case with $C = 1$.

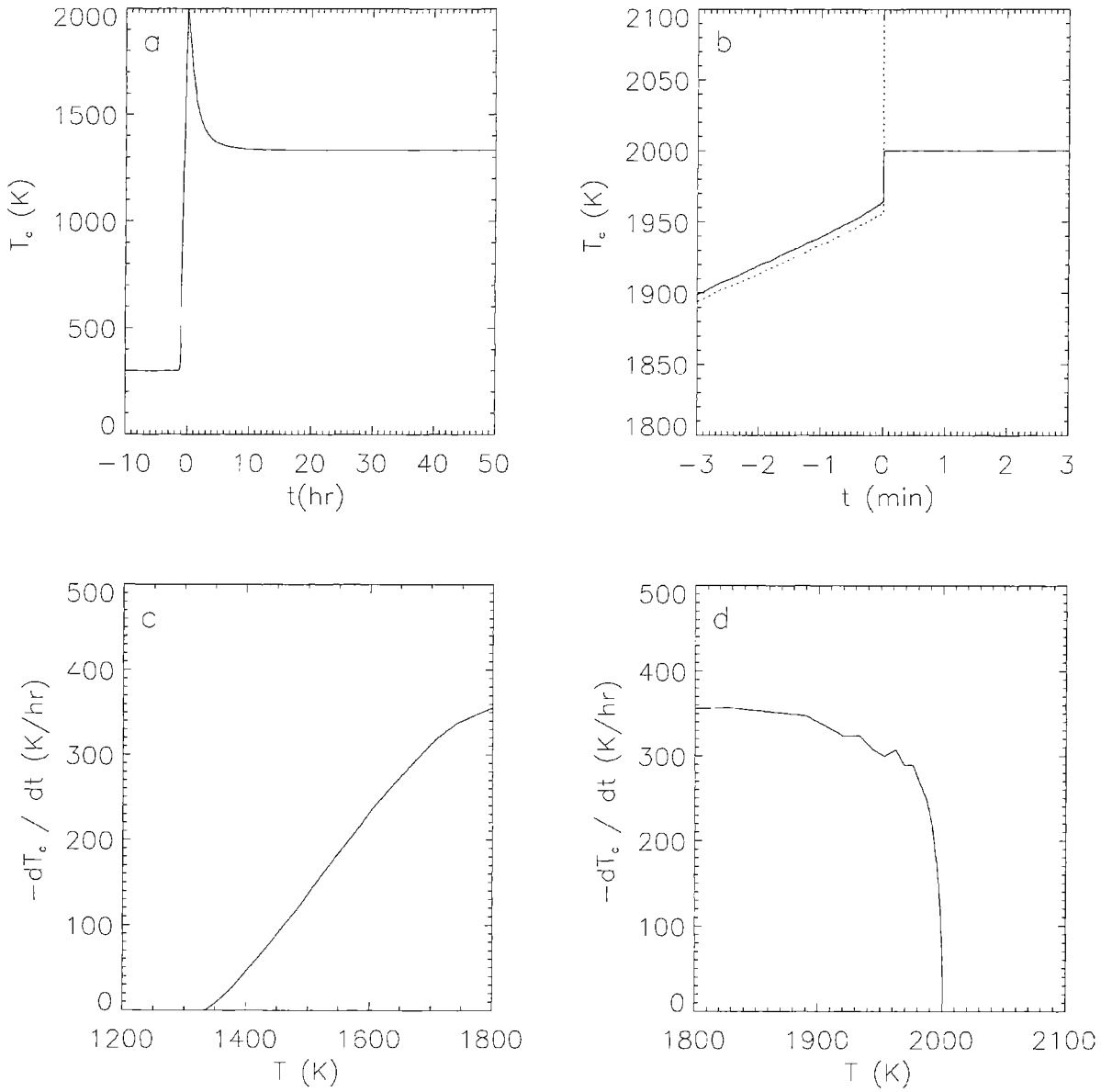

FIG. 6. Same as Fig. 4, but with chondrule concentration increased by a factor of 300 over the canonical "solar" value ($C = 300$). Note the changed abscissas and ordinates to accomodate the higher peak temperatures and cooling rates. The cooling rate at high temperatures (d) has been reduced because chondrules spend their entire gas-drag heating stage at temperatures high enough (2000 K) to be evaporating instead of heating or cooling.

regions with C less than some critical value about 10–100, and only in those regions. Chondrules with barred and radial textures must have formed in regions with $C \gtrsim 10$–100, and only in those regions.

DISCUSSION

Cooling Rates

One of the most important predictions of the shock wave model is of a generally positive correlation between the cooling rate through crystallization temperatures (~1600 K) and the chondrule number density. To simplify the discussion, we derive a formula relating the cooling rate to the physical inputs and show it is consistent with our numerical results. We assume that after the initial gas-drag heating stage, the temperatures of the gas and dust are well coupled. The gas cools by thermal exchange with chondrules, so if chondrules remain hot, the gas cannot cool. Likewise, chondrules are kept hot by thermal contact with the gas, so if the gas remains hot, so will the chondrules. Together, the chondrules and gas cool only as fast as the chondrules and the gas (through the dust component)

TABLE 5. Variation in peak temperature and cooling rate due to density and shock speed.

Density ρ_{gas} (g cm^{-3})	Shock speed, V_s (km/s)				
	5	6	7	8	9
3×10^{-10}	1119 K N/A	1321 K N/A	1512 K N/A	1695 K ~10^4 K h^{-1}	1896 K 22 K h^{-1}
1×10^{-9}	1299 K N/A	1582 K N/A	1858 K 50 K h^{-1}	2000 K 292 μm* 5 K h^{-1} dust evap.	2000 K 0 μm* N/A dust evap.
3×10^{-9}	1443 K N/A	1795 K 120 K h^{-1}	2000 K 294 μm* 12 K h^{-1} dust evap.	2000 K 0 μm* N/A dust evap.	2000 K 0 μm* N/A dust evap.

*At 2000 K, chondrule is assumed to evaporate. Final chondrule radius (μm) is given.

can radiate away their combined heat energy. This requires them to travel several optical depths from the shock front, or else the chondrules and gas (dust) will absorb radiation as fast as they emit it. The cooling rate of a chondrule is essentially its temperature drop, ~300 K, divided by the timescale for its temperature to drop. This timescale is a factor of 4 greater than the timescale to escape the radiation from the shock, because chondrule heating and cooling scale as T_c^4. The cooling timescale is therefore

$$t_{cool} \approx 4\frac{\Delta\tau}{\rho_g V_g \kappa} \approx 7 \text{ h} \quad (36)$$

where $\kappa \approx 1.14\ (1 + C/50)$ cm^2 g^{-1} is the opacity and $\Delta\tau \approx 5$ is the number of optical depths that must be crossed to escape the radiation of the shock front. This yields a cooling rate

$$\text{CR} \approx 50\left(\frac{\rho_{gas}}{10^{-9}\text{ g cm}^{-3}}\right)\left(\frac{V_s}{7\text{ km s}^{-1}}\right)\left(\delta + \frac{C}{50}\right) \text{K h}^{-1} \quad (37)$$

where $\delta = 1$ if dust has not evaporated, and $\delta = 0$ if it has.

This formula reproduces the cooling rates of chondrules very well in all cases where the dust does not evaporate. For the series of cases with $\rho_{gas} = 1 \times 10^{-9}$ g cm^{-3}, $V_s = 7$ km s^{-1} and $C \leq 100$ (Table 4), Eq. (37) is accurate to within 10%; this formula underestimates the cooling rate for $C = 300$, predicting 300 K h^{-1} instead of 400 K h^{-1}. Equation (37) predicts well the cooling rates for the cases $\rho_{gas} = 3 \times 10^{-10}$ g cm^{-3}, $V_s = 9$ km s^{-1}, $C = 1$ (19 K h^{-1} instead of 22 K h^{-1}), and $\rho_{gas} = 3 \times 10^{-9}$ g cm^{-3}, $V_s = 7$ km s^{-1}, $C = 1$ (129 K h^{-1} instead of 120 K h^{-1}). The formula tends to overestimate the cooling rate in the two cases for which the chondrule density was not enhanced and yet dust evaporated. Equation (37) would predict a cooling rate of only 1 K h^{-1} for the case with $\rho_{gas} = 1 \times 10^{-9}$ g cm^{-3}, $V_s = 8$ km s^{-1} and $C = 1$, instead of the calculated 5 K h^{-1}; likewise, it would predict only 3 K h^{-1} for the case with $\rho_{gas} = 1 \times 10^{-9}$ g cm^{-3}, $V_s = 8$ km s^{-1} and $C = 1$, instead of the calculated 12 K h^{-1}. An analysis of the cooling curves in these two cases reveals that the basic assumption of Eq. (37), namely that the gas and particles are thermally well coupled, breaks down when the dust evaporates. When dust is present, it couples the gas and particles during the cooling stage so that their temperatures differ by <1 K, but when dust is evaporated, the remaining chondrules and the gas have temperature differences of 5–10 K. This changes the energetics enough so that the cooling rates in the two odd cases just discussed are about a factor of 4 too low. Still, in all cases, Eq. (37) gives a good qualitative sense of the variation of cooling rate with input conditions, and is numerically very accurate in those cases where dust does not evaporate. It also clearly demonstrates that cooling rates $\gtrsim$100 K h^{-1} are possible only for very high concentrations of chondrules ($C \gtrsim 100$), or very high mass densities $\rho_{gas} \gtrsim 3 \times 10^{-9}$ g cm^{-3}), both conditions implying a high spatial density of chondrules.

Compound Chondrules

Above we have demonstrated a break in the cooling rates at $C \approx 30$. As Table 4 shows, a second break exists, in the peak temperatures experienced by chondrules. Roughly, if $C \gtrsim 300$, then the peak temperatures are high enough to completely melt the chondrule and even induce evaporation, while if $C \lesssim 100$, the chondrule is mostly, but incompletely melted. That is to say, chondrules from regions with $C \lesssim 100$ will necessarily be porphyritic, while chondrules from regions with $C \gtrsim 100$ will have cooling rates characteristic of barred olivines, and will be completely melted as well. Numerical simulations of turbulent concentration suggest that chondrules spend ~20% of their time in regions with $C > 10^2$, and that these regions make up ~10^{-3}

of the volume of the nebula (Cuzzi *et al.*, 2001). As such, ~80% of all chondrules should be caught in regions with $C < 100$ when overtaken by a shock wave, and end up being porphyritic. The other 20% should be completely melted and end up with either barred or radial textures. This fraction agrees well with the fraction of chondrules in the general population that are porphyritic (84%), and radial (7–9%) or barred (3–4%) (Gooding and Keil, 1981).

We can also use these results to estimate the frequency of compound chondrules and to predict what their textures should be. Compound chondrules make up ~2.4% of all chondrules in ordinary chondrites (Wasson *et al.*, 1995). Compound chondrules result when two (or more) chondrules collide, at least one of which is still plastic so that the two stick. The minimum temperature for being plastic is ~1400 K (Connolly *et al.*, 1994). The probability of a collision per unit timescales as the product of the square of the chondrule concentration C and the plasticity times (time during which the chondrule temperature exceeds 1400 K). The plasticity times computed numerically here, $t_{\rm plast} \approx 10^4$ s, are roughly independent of C, to within factors ~3. Following Gooding and Keil (1981), we estimate the probability a given chondrule will stick to a second chondrule to be

$$P_{\rm comp} = \sqrt{2}\, 4\pi a_{\rm c}^2 V_{\rm rel} n_{\rm c} t_{\rm plast} \qquad (38)$$

where $V_{\rm rel}$ is the relative velocity between chondrules and $n_{\rm c}$ is their spatial number density. The relative velocity between chondrules in a turbulent solar nebula with $\alpha = 10^{-4}$ has been shown to be ~100 cm s^{-1} (Cuzzi *et al.*, 1998), and we use a post-shock gas density of 10^{-8} g cm^{-3}. The frequency of compound chondrules can then be reproduced (*i.e.*, $P_{\rm comp} = 0.024$) if the average concentration of chondrules is $C \approx 15$, which is entirely consistent with the known result that the average concentration of chondrules will greatly exceed unity. We note that if chondrules were to spend 80% of their time in regions with $C = 1$ and 20% of their time in regions with $C = 100$, their average concentration would be 21. Further work is planned to quantify these predictions, but turbulent concentration and the shock model presented here appear capable of explaining the frequency of compound chondrules.

The textures of compound chondrules can be explained as well. Compound chondrules are much more likely to be formed in regions of very high C. Specifically, a region with $C = 100$ will produce $10^4\times$ as many compound chondrules (per unit volume) as a $C = 1$ region. Even if such regions make up only a fraction 10^{-3} of the volume (Cuzzi *et al.*, 2001), compound chondrules will overwhelmingly sample high-C (specifically, $C \gtrsim 100$) chondrule formation conditions. Thus, compound chondrules should be predominantly radial and barred. These conclusions are consistent with the data presented by Wasson *et al.* (1995), who compiled statistics on the number of compound chondrules with different textures. We restrict our attention to the subset of their data that are barred, porphyritic or radial, since these make up the bulk of their data. Compound chondrules are overwhelmingly fully melted (radial or barred textures) rather than partially melted (porphyritic textures), compared to the general chondrule population. In the general chondrule population, (barred + radial)/(barred + radial + porphyritic) ≈ 13% (Gooding and Keil, 1981), while among the compound chondrules studied by Wasson *et al.* (1995), (barred + radial)/(barred + radial + porphyritic) = (44 + 64)/(44 + 64 + 26) = 81%. If radial textures are classified as fast coolers, then the same proportions demonstrate that compound chondrules are also fast coolers. If radial textures are discarded in favor of the more tightly constrained cooling rates of barred and porphyritic textures, the same conclusion is reached. Among the general population, barred/(barred + porphyritic) = 5% (Gooding and Keil, 1981), while among the compound chondrules studied by Wasson *et al.* (1995), barred/(barred + porphyritic) = 44/(44 + 26) = 63%. Clearly, compound chondrules are fast coolers and are more often fully melted than chondrules in the general population. Since compound chondrules almost certainly formed by collisions in regions of higher chondrule density, these data clearly support the conclusion that high chondrule densities are correlated positively with degree of melting and cooling rate. This correlation is predicted by the shock model presented here.

We point out that other models of chondrule formation do not make this prediction, or would even come to the opposite conclusion. Models in which chondrule peak temperatures are controlled by an external energy source, such as exposure to sunlight (Shu *et al.*, 1996; Eq. (11)) would either predict no correlation between the degree of melting and chondrule density, or would predict a lower degree of melting, because the same energy is distributed among more chondrules or because chondrules shield each other from the energy source. Likewise, if the chondrule temperature is controlled by the decay of an external energy source (*e.g.*, the drop in irradiation following a flare), then there would be no correlation of cooling rate with the chondrule density. More significantly, if the chondrule temperature were determined by the diffusion of radiation through an optically thick slab of chondrules (*e.g.*, Sahagian and Hewins, 1992; Hood and Horanyi, 1993; Hood and Kring, 1996; Hood and Ciesla, 2001), then the cooling rates should be *lower* for higher chondrule densities, opposite to the conclusion reached in this paper, and in contradiction with the meteoritic evidence.

Pre-Shock Heating

An inevitable consequence of any shock model is that hot chondrules that have just passed through the shock front will emit radiation that will be absorbed by chondrules before reaching the shock front (Desch and Connolly, 2001). To the extent that the gas density and shock speed are fixed, the time for which the chondrule will be heated before passing through the shock is more or less fixed. In the canonical run presented here, chondrules were above 500 K for ~230 min, above 1000 K

for ~170 min, and above 1500 K for ~64 min, before reaching temperatures of 1742 K just before being shocked. The gas-drag heating that ensued was enough to heat the chondrules to 1858 K, and the chondrules then cooled rapidly (~10^4 K h^{-1}) to a baseline temperature of ~1730 K, thereafter cooling at $\lesssim 10^2$ K h^{-1}. The partial melting of chondrules before they even reach the shock front may be essential to their survival in shocks if chondrule precursors were fragile aggregates. Still, the question arises as to whether primary sulfides could be retained during the prolonged pre-shock heating. The sulfides observed by Rubin *et al.* (1999) were asserted to be primary because they were sited within large silicate phenocrysts, and had to have been housed in silicate crystals before and during melting. Chondrules with troilite sited within large crystals would not have lost the sulfides during the hours before passage of our canonical shock, because the chondrules did not heat above 1750 K, and would have been only partially melted. After passing through the shock, peak temperatures are sufficient to completely melt chondrules, but retention at this stage depends on the kinetics of the melting and diffusion. It is at this point that the experiments of Yu *et al.* (1996) and Yu and Hewins (1998) become relevant: sulfur could still be retained, even with peak temperatures ~250 K above the liquidus, provided the initial cooling rates exceeded ~5000 K h^{-1}. These conditions are satisfied by the shock model presented here, and so we assert that the long stage of pre-shock heating would not necessarily lead to loss of volatiles.

Remanent Magnetization

Both chondrites and chondrules contain remanent magnetizations that can be used to infer the paleofields of their formation environments. Many uncertainties accompany the following derived paleofields (Wasilewski and Dickinson, 1995, 2000), but we will accept them and conclude that chondrules experienced stronger magnetic fields than their parent chondrites. Assuming that the remanent magnetizations are due to thermoremanent magnetization, several carbonaceous chondrites, including Allende, were exposed to paleofields ~1.0 ± 0.3 G (Nagata, 1979). Ordinary chondrites were exposed to paleofields estimated as about 0.01–0.1 G (Brecher and Leung, 1979), to ~0.1 G (Nagata, 1979), to ~0.2 G (Gus'kova, 1963; Herndon *et al.*, 1972), up to 0.7–1.4 G (Westphal and Whitechurch, 1983). Generally, chondrites are supposed to record magnetic fields about 0.1–1 G (Stacey *et al.*, 1961; Herndon and Rowe, 1974). This is consistent with estimates of the magnetic field strength of the early solar system of 0.1–1 G (Nakano and Umebayashi, 1986; Desch, 1998; Desch and Mouschovias, 2001), due to magnetic field lines being dragged in from the molecular cloud during collapse of the molecular cloud core. The formation of chondrules and of chondrites are each predicted to take place amid the backdrop of a uniform, dynamically weak magnetic field, oriented perpendicular to the disk. Chondrites would naturally record this background field. Chondrules would also be exposed to this magnetic field, yet they record magnetic field strengths an order of magnitude greater than their host chondrites, about 1–10 G (Levy, 1988; Wasilewski and O'Bryan, 1994; Jones *et al.*, 2000). In Allende, chondrules were exposed to paleofields estimated as 2–7 G (Lanoix *et al.*, 1978b), and 2–16 G (Lanoix *et al.*, 1978). The magnetizations of chondrules within chondrites are randomly oriented, suggesting they were magnetized individually before incorporation into chondrites (Sugiura *et al.*, 1979). It is presumed that chondrules acquired their magnetization as they cooled through their Curie points (presumably of kamacite, $T_{\rm curie} \approx 1040$ K) following the chondrule formation event.

If chondrules were melted in shocks, they would have cooled through their Curie points while still in a shock-compressed gas. If magnetic field lines were initially oriented parallel to the shock front (*i.e.*, field lines normal to the disk, with the shock propagating in the disk), then field lines would be compressed by the shock, assuming that the hot, shocked gas was sufficiently ionized to couple to the magnetic field on timescales of tens of hours. The compression of the field lines would scale with the density (*e.g.*, Shore, 1992), so the factor by which the gas is compressed also would be the ratio between the magnetic field seen by chondrules and the background magnetic field seen by chondrites. This factor is ~11 in our canonical run, so that if chondrites experienced field strengths about 0.1–1.0 G, chondrules would naturally acquire magnetizations from fields about 1–10 G in strength.

Source of Nebula Shocks

The canonical run presented here assumed ambient densities of 1×10^{-9} g cm^{-3} and ambient temperatures on the order of 300 K. These values are consistent with a protoplanetary disk that is gravitationally unstable beyond 5 AU, but (locally) stable inward of 5 AU (Bell *et al.*, 1997). The mass accretion rate needed to produce a disk this massive, 10^{-8} $M_\odot$ $year^{-1}$, is the median mass accretion rate of T Tauri stars 1 Ma old of age, although mass accretion rates this high have been found in T Tauri systems that are 2–3 Ma old (Fig. 3a of Hartmann *et al.*, 1998). The evolution of protoplanetary disks that are marginally gravitationally unstable at 5–20 AU has been investigated by Boss (2001) in the context of forming Jupiter by gravitational collapse rather than core accretion. Clumps are found to form on timescales ~10^5 years, which may possibly be gravitationally bound but may also be sheared apart. While the clumps exist, however, they tend to drive associated density structures at radii interior to them, that are oriented normal to the orbital flow (Boss, 2000). These structures have a tendency to co-orbit with the dense clumps driving them, and gas at smaller radii will collide with the structures with relative velocities ~10 km s^{-1} (Boss, 2000). For example, gas orbiting at 2.5 AU would overtake the density structures at a relative velocity equal to the difference in orbital velocities between the gas at 2.5 AU ($V_{\rm K}$ = 19 km s^{-1})

and the clump, at ~6 AU (V_K = 12 km s^{-1}). Gas in the asteroid belt is therefore expected to encounter the density structures as a 7 km s^{-1} shock. In one numerical simulation, the actual velocity difference between the density structure and gas at 4.5 AU was found to be 7 km s^{-1} (Boss, 2001, pers. comm.). Numerical simulations extending the inner grid boundary to 2 AU (from 4 AU) are planned (Boss, 2002; unpubl. data), which should verify the presence of shocks in the asteroid belt region and provide statistics on the frequency and intensity of shocks. Nonetheless, it seems plausible that while the protoplanetary disk remains massive, for about 1–3 Ma, shocks should be generated that are capable of melting chondrules. These shocks would be repeatable, since clumps may form and shear apart and form again, but only stochastically.

CONCLUSIONS

During the first few million years of the solar system's evolution, mass accretion rates were high enough ($\gtrsim 10^{-8}$ $M_\odot$ year^{-1}; Hartmann *et al.*, 1998) that the nebula could have been gravitationally unstable beyond 5 AU (Bell *et al.*, 1997). Gravitational instabilities in these regions could create overdense regions that would sweep through the protoplanetary disk at radii <5 AU, with high (~7 km s^{-1}) velocities relative to the gas there (Boss, 2000, 2001). Such gravitational instabilities would probably manifest themselves as shocks, capable of melting chondrules (Boss, 2000). In this paper we have modeled the thermal histories of particles as they pass through shock waves, taking into account the transfer of radiation, the dissociation of hydrogen, and evaporation of dust and/or chondrules. We find that peak temperatures sufficient to melt chondrules are produced in the shock waves that plausibly swept through the nebula. Moreover, we have reproduced the cooling rates of porphyritic chondrules with the assumption that a fraction of the solid material in a solar composition gas is in the form of chondrules. The cooling rates are nonlinear, being very rapid above the liquidus (~10^4 K h^{-1}) and moderate (~50 K h^{-1}) over the crystallization temperature range. The fast cooling rates above the liquidus are consistent with constraints imposed at high temperatures by the retention of sulfur (Yu *et al.*, 1996), and the cooling rates at lower temperatures are consistent with the many cooling rates in the literature, which we have reviewed here. These results are robust in that chondrules melted by shocks of any strength or gas density will have similar cooling rates.

It is also quite likely that chondrules were concentrated into small regions by turbulence in the solar nebula (Cuzzi *et al.*, 2001). The faster cooling rates and higher peak temperatures of barred and radial chondrules are reproduced naturally by the shock model if those chondrules come from regions with a higher chondrule-to-gas ratio ($C \gtrsim 100$). *This positive correlation between chondrule density and cooling rate and peak temperature is a unique prediction of the shock model presented here, and is supported by the overrepresentation of barred and radial textures among compound chondrules.* Assuming chondrule concentrations vary due to turbulent concentration according to the probability distribution functions of Cuzzi *et al.* (2001), we estimate that ~80% of all chondrules should be porphyritic, a number that compares well with observations (Gooding and Keil, 1981). Combining the relative velocities and average concentrations of chondrules from the turbulent concentration model with the plasticity times computed here also reproduces well the frequency of compound chondrules. The shock wave model also predicts that the remanent magnetizations of chondrules should be an order of magnitude greater than those of their parent chondrites, in accord with observations.

Future work will quantify the statistical distributions of shock speeds and gas densities and chondrule concentrations, allowing predictions of how often a chondrule will actually experience a 7 km s^{-1} shock, and of the statistics of chondrule textures. We also plan to refine the calculations done here to include line cooling due to H_2O emission, to quantify how quickly the gas cools on its own; this may set a lower bound on the chondrule cooling rates. The shock wave model also inevitably predicts that chondrules are heated above 1000 K for hours before they even reach the shock front; volatile loss should be studied in this context. Despite these areas of future work, it is encouraging that the shock wave model provides a context for studying chondrule formation. The many compelling consistencies between the meteoritic record and the predictions of the model presented here bring us to the conclusion that chondrules formed in the solar nebula by passing through shock waves.

Acknowledgments–We would like to thank Alan Boss for making available his calculations and aiding in our understanding of solar nebula shocks, Jeff Cuzzi, Conel Alexander, Pat Cassen and Dottie Woolum for helping us to refine some of the issues regarding chondrule formation, Michael Kaufman for aiding in our understanding of the transfer of line radiation, and Danielle Moser for assisting in the calculations of compound chondrule textures. S. J. D. was supported by a NASA Astrobiology Grant and by a Carnegie Fellowship during this work.

Editorial handling: P. Cassen

REFERENCES

BELL K. R., CASSEN P. M., KLAHR H. H. AND HENNING TH. (1997) The structure and appearance of protostellar accretion disks: Limits on disk flaring. *Astrophys. J.* **486**, 372–387.

BOSS A. P. (1996) A concise guide to chondrule formation models. In *Chondrules and the Protoplanetary Disk* (eds. R. H. Hewins, R. H. Jones and E. R. D. Scott), pp. 257–263. Cambridge Univ. Press, New York, New York, USA.

BOSS A. P. (2000) Shock wave heating and clump formation in a minimum mass solar nebula (abstract). *Lunar Planet. Sci.* **31**, #1084, Lunar and Planetary Institute, Houston, Texas, USA (CD-ROM).

BOSS A. P. (2001) Formation of planetary-mass objects by protostellar collapse and fragmentation. *Astrophys. J.* **551**, L167–L170.

BOSS A. P. AND GRAHAM J. A. (1993) Clumpy accretion and chondrule formation. *Icarus* **106**, 168–178.

BRECHER A. AND LEUNG L. (1979) Ancient magnetic field determinations on selected chondritic meteorites. *Phys. Earth Planet. Int.* **20**, 361–378.

CHERCHNEFF I., BARKER J. R. AND TIELENS A. G. G. M. (1992) Polycyclic aromatic hydrocarbon formation in carbon-rich stellar atmospheres. *Astrophys. J.* **401**, 269–287.

CIESLA F. J. AND HOOD L. L. (2001) Chondrule formation by passage of a shock through a dust-gas suspension (abstract). *Lunar Planet. Sci.* **32**, #1367, Lunar and Planetary Institute, Houston, Texas, USA (CD-ROM).

COHEN B. A., HEWINS R. H. AND YU Y. (2000) Evaporation in the young solar nebula as the source of "just-right" melting of chondrules. *Nature* **406**, 600–602.

CONNOLLY H. C., JR. AND HEWINS R. H. (1991) The influence of bulk composition and dynamic melting conditions on olivine chondrule textures. *Geochim. Cosmochim. Acta* **55**, 2943–2950.

CONNOLLY H. C., JR. AND HEWINS R. H. (1995) Chondrules as products of dust collisions with totally molten droplets within a dust-rich nebular environment: An experimental investigation. *Geochim. Cosmochim. Acta* **59**, 3231–3246.

CONNOLLY H. C., JR. AND LOVE S. G. (1998) The formation of chondrules: Petrologic tests of the shock wave model. *Science* **280**, 62–67.

CONNOLLY H. C., JR., HEWINS R. H., ATRA N. AND LOFGRE G. E. (1994) Compound chondrules: An experimental investigation (abstract). *Meteoritics* **29**, 458.

CONNOLLY H. C., JR., JONES B. D. AND HEWINS R. H. (1998) The flash heating of chondrules: An experimental investigation into the melting history and physical nature of chondrule precursors. *Geochim. Cosmochim. Acta* **62**, 2725–2735.

CUZZI J. N., DOBROVOLSKIS A. R. AND HOGAN R. C. (1996) Turbulence, chondrules, and planetesimals. In *Chondrules and the Protoplanetary Disk* (eds. R. H. Hewins, R. H. Jones and E. R. D. Scott), pp. 35–44. Cambridge Univ. Press, New York, New York, USA.

CUZZI J. N., HOGAN R. C., PAQUE J. M. AND DOBROVOLSKIS A. R. (1998) Chondrule rimming by sweepup of dust in the protoplanetary nebula: Constraints on primary accretion (abstract). *Lunar Planet. Sci.* **29**, #1439, Lunar and Planetary Institute, Houston, Texas, USA (CD-ROM).

CUZZI J. N., HOGAN R. C., PAQUE J. M. AND DOBROVOLSKIS A. R. (2001) Size-selective concentration of chondrules and other small particles in protoplanetary nebula turbulence. *Astrophys. J.* **546**, 496–508.

DEHART J. M. AND LOFGREN G. E. (1996) Experimental studies of group A1 chondrules. *Geochim. Cosmochim. Acta* **60**, 2233–2242.

DESCH S. J. (1998) The magnetic decoupling stage of star formation. Ph.D. thesis, Univ. Illinois, Urbana-Champaign, Illinois, USA. 195 pp.

DESCH S. J. (2000) Astrophysical constraints on chondrule formation models (abstract). *Lunar Planet. Sci.* **31**, #1923, Lunar and Planetary Institute, Houston, Texas, USA (CD-ROM).

DESCH S. J. AND CONNOLLY H. C., JR. (2001) Melting of chondrules and type B CAIs by nebula shocks (abstract). *Lunar Planet. Sci.* **32**, #2163, Lunar and Planetary Institute, Houston, Texas, USA (CD-ROM).

DESCH S. J. AND CUZZI J. N. (2000) The generation of lightning in the solar nebula. *Icarus* **143**, 87–105.

DESCH S. J. AND MOUSCHOVIAS T. CH. (2001) The magnetic decoupling stage of star formation. *Astrophys. J.* **550**, 314–333.

DRAINE B. T. AND LEE H. M. (1984) Optical properites of interstellar graphite and silicate grains. *Astrophys. J.* **285**, 89–108.

GOMBOSI T. I., NAGY A. F. AND CRAVENS T. E. (1986) Dust and neutral gas modeling of the inner atmospheres of comets. *Rev. Geophys.* **24**, 667–700.

GOODING J. L. AND KEIL K. (1981) Relative abundances of chondrule primary textural types in ordinary chondrites and their bearing on conditions of chondrule formation. *Meteoritics* **16**, 17–43.

GUSKOVA E. G. (1963) Investigation of natural remanent magnetization of stony meteorites. *Geomagnetism Aeronomy* **3**, 308–312.

HARTMANN L., CALVET N., GULLBRING E. AND D'ALESSIO P. (1998) Accretion and the evolution of T Tauri disks. *Astrophys. J.* **495**, 385–400.

HAYASHI C. (1981) Structure of the solar nebula, growth and decay of magnetic fields and effects of magnetic and turbulent viscosities on the nebula. *Prog. Theor. Phys. Suppl.* **70**, 35–53.

HENNING TH. AND STOGNIENKO R. (1996) Dust opacities for protoplanetary accretion disks: Influence of dust aggregates. *Astron. Astrophys.* **311**, 291–303.

HERNDON J. M. AND ROWE M. W. (1974) Magnetism in meteorites. *Meteoritics* **9**, 289–305.

HERNDON J. M., ROWE M. W., LARSON E. E. AND WATSON D. E. (1972) Magnetism of meteorites: A review of Russian studies. *Meteoritics* **7**, 263–284.

HEWINS R. H. (1996) Chondrules and the protoplanetary disk: An overview. In *Chondrules and the Protoplanetary Disk* (eds. R. H. Hewins, R. H. Jones and E. R. D. Scott), pp. 3–9. Cambridge Univ. Press, New York, New York, USA.

HEWINS R. H. (1997) Chondrules. *Ann. Rev. Earth. Planet. Sci.* **25**, 61–83.

HEWINS R. H. AND CONNOLLY H. C., JR. (1996) Peak temperatures of flash-melted chondrules. In *Chondrules and the Protoplanetary Disk* (eds. R. H. Hewins, R. H. Jones and E. R. D. Scott), pp. 197–204. Cambridge Univ. Press, New York, New York, USA.

HEWINS R. H., KLEIN L. C. AND FASANO B. V. (1981) Conditions of formation of pyroxene excentroradial chondrules (abstract). *Lunar Planet. Sci.* **7**, 448–450.

HEWINS R. H., ZANDA B., HORANYI M., ROBERTSON S., DEN HARTOG D. J. AND FIKSEL G. (2000) The trouble with flash-heating (abstract). *Lunar Planet. Sci.* **31**, #1675, Lunar and Planetary Institute, Houston, Texas, USA (CD-ROM).

HOLLENBACH D. J. AND MCKEE C. F. (1979) Molecule formation and infrared emission in fast interstellar shocks. I. Physical processes. *Astrophys. J. Suppl.* **41**, 555–592.

HOOD L. L. (1998) Thermal processing of chondrule and CAI precursors in planetesimal bow shocks. *Meteorit. Planet. Sci.* **33**, 97–107.

HOOD L. L. AND CIESLA F. J. (2001) The nebular shock wave model for chondrule formation: Constraints imposed by chondrule cooling rates (abstract). *Lunar Planet. Sci.* **32**, #1986, Lunar and Planetary Institute, Houston, Texas, USA (CD-ROM).

HOOD L. L. AND HORANYI M. (1991) Gas dynamic heating of chondrule precursor grains in the solar nebula. *Icarus* **93**, 259–269.

HOOD L. L. AND HORANYI M. (1993) The nebula shock wave model for chondrule formation—One-dimensional calculations. *Icarus* **106**, 179–189.

HOOD L. L. AND KRING D. A. (1996) Models for multiple heating mechanisms. In *Chondrules and the Protoplanetary Disk* (eds. R. H. Hewins, R. H. Jones and E. R. D. Scott), pp. 257–263. Cambridge Univ. Press, New York, New York, USA.

HORANYI M. AND ROBERTSON S. (1996) Chondrule formation in lightning discharges: Status of theory and experiment. In *Chondrules and the Protoplanetary Disk* (eds. R. H. Hewins, R. H. Jones and E. R. D. Scott), pp. 303–310. Cambridge Univ. Press, New York, New York, USA.

HOWARD E. (1802) Experiments and observations on certain stony substances, which at different times are said to have fallen on the Earth; also on various kinds of native iron. *Phil. Trans. Royal Soc. London* **92**, 168–212.

HUSS G. R. (1988) The role of presolar dust in the formation of the solar system. *Earth Moon Planets* **40**, 165–211.

JONES R. H. AND LOFGREN G. E. (1993) A comparison of FeO-rich, porphyritic olivine chondrules in unequilibrated ordinary chondrites and experimental analogues. *Meteoritics* **28**, 213–221.

JONES R. H., LEE T., CONNOLLY H. C., JR., LOVE S. G. AND SHANG H. (2000) Formation of chondrules and CAIs: Theory *vs.* observations. In *Protostars and Planets IV* (eds. V. Mannings, A. P. Boss and S. S. Russell), pp. 927–962. Univ. Arizona Press, Tucson, Arizona, USA.

KENNEDY A. K., LOFGREN G. E. AND WASSERBURG G. J. (1993) An experimental study of trace element partitioning between olivine, orthopyroxene and melt in chondrules—Equilibrium values and kinetic effects. *Earth Planet. Sci. Lett.* **115**, 177–195.

KIPPENHAHN R. AND WEIGERT A. (1990) *Stellar Structure and Evolution*. Springer-Verlag, Berlin, Germany. 468 pp.

LANOIX M., STRANGWAY D. W. AND PEARCE G. W. (1978a) The primordial magnetic field preserved in chondrules of the Allende meteorite. *Geophys. Res. Lett.* **5**, 73–76.

LANOIX M., STRANGWAY D. W. AND PEARCE G. W. (1978b) Paleointensity determinations from Allende chondrules. *Proc. Lunar Planet. Sci. Conf.* **9th**, 630–632.

LARSON R. B. (2002) The role of tidal interactions in star formation. *Mon. Not. Royal Astron. Soc.* (in press).

LEVY E. H. (1988) Energetics of chondrule formation. In *Meteorites and the Early Solar System* (eds. J. F. Kerridge and M. S. Matthews), pp. 697–714. Univ. Arizona Press, Tucson, Arizona, USA.

LIFFMAN K. AND BROWN M. J. I. (1996) The protostellar jet model of chondrule formation. In *Chondrules and the Protoplanetary Disk* (eds. R. H. Hewins, R. H. Jones and E. R. D. Scott), pp. 285–302. Cambridge Univ. Press, New York, New York, USA.

LIFFMAN K. AND TOSCANO M. (2000) Chondrule fine-grained mantle formation by hypervelocity impact of chondrules with dusty gas. *Icarus* **143**, 106–125.

LOFGREN G. E. (1989) Dynamic crystallization of chondrule melts of porphyritic olivine composition—Textures experimental and natural. *Geochim. Cosmochim. Acta* **53**, 461–470.

LOFGREN G. E. AND LANIER A. B. (1990) Dynamic crystallization study of barred olivine chondrules. *Geochim. Cosmochim. Acta* **54**, 3537–3551.

LOFGREN G. E. AND LE L. (1996) Thermal recycling of chondrules: I. Experimental study of remelting on texture (abstract). *Lunar Planet. Sci.* **27**, 765.

LOFGREN G. AND RUSSELL W. J. (1986) Dynamic crystallization of chondrule melts of porphyritic and radial pyroxene composition. *Geochim. Cosmochim. Acta* **50**, 1715–1726.

MACPHERSON G. J., WARK D. A. AND ARMSTRONG J. T. (1988) Primitive material surviving in chondrites: Refractory inclusions. In *Meteorites and the Early Solar System* (eds. J. F. Kerridge and M. S. Matthews), pp. 746–807. Univ. Arizona Press, Tucson, Arizona, USA.

MCSWEEN H. Y., JR. (1977) Chemical and petrographic constraints on the origin of chondrules and inclusions in carbonaceous chondrites. *Geochim. Cosmochim. Acta* **41**, 1843–1860.

MIHALAS D. (1978) *Stellar Atmospheres*. W. H. Freeman & Co., San Francisco, California, USA. 650 pp.

MIHALAS D. AND MIHALAS B. W. (1985) *Foundations of Radiation Hydrodynamics*. Oxford Univ. Press, Oxford, U.K. 718 pp.

MORFILL G. E., DURISEN R. H. AND TURNER G. W. (1998) Note: An accretion rim constraint on chondrule formation theories. *Icarus* **134**, 180–184.

NAGATA T. (1979) Meteorite magnetism and the early solar system magnetic field. *Phys. Earth Planet. Int.* **20**, 324–341.

NAKANO T. AND UMEBAYASHI T. (1986) Dissipation of magnetic fields in very dense interstellar clouds. II. Final phases of star formation and the magnetic flux of a newborn star. *Mon. Not. Royal Astron. Soc.* **221**, 319–338.

NEUFELD D. A. AND KAUFMAN M. J. (1993) Radiative cooling of warm molecular gas. *Astrophys. J.* **418**, 263–272.

OSSENKOPF V. AND HENNING TH. (1994) Dust opacities for protostellar cores. *Astron. Astrophys.* **291**, 943–959.

PALME H., SPETTEL B. AND IKEDA Y. (1993) Origin of chondrules and matrix in carbonaceous chondrites (abstract). *Meteoritics* **28**, 417.

PILIPP W., HARTQUIST T. W., MORFILL G. E. AND LEVY E. H. (1998) Chondrule formation by lightning in the protosolar nebula? *Astron. Astrophys.* **331**, 121–146.

PROBSTEIN R. F. (1968) In *Problems of Hydrodynamics and Continuum Mechanics*, p. 568. Society Industrial Applied Mathematics, Philadelphia, Pennsylvania, USA.

RADOMSKY P. M. AND HEWINS R. H. (1990) Formation conditions of pyroxene-olivine and magnesian olivine chondrules. *Geochim. Cosmochim. Acta* **54**, 3475–3490.

RUBIN A. E., SAILER A. L. AND WASSON J. T. (1999) Troilite in the chondrules of type-3 ordinary chondrites: Implications for chondrule formation. *Geochim. Cosmochim. Acta* **63**, 2281–2298.

RUZMAIKINA T. M. AND IP W. H. (1994) Chondrule formation in radiative shock. *Icarus* **112**, 430–447.

SAHAGIAN D. L. AND HEWINS R. H. (1992) The size of chondrule-forming events (abstract). *Lunar Planet. Sci.* **23**, #1197, Lunar and Planetary Institute, Houston, Texas, USA (CD-ROM).

SEARS D. W. G., HUANG S. AND BENOIT P. H. (1996) Open-system behavior during chondrule formation. In *Chondrules and the Protoplanetary Disk* (eds. R. H. Hewins, R. H. Jones and E. R. D. Scott), pp. 221–231. Cambridge Univ. Press, New York, New York, USA.

SHORE S. N. (1992) *An Introduction to Astrophysical Hydrodynamics*. Academic Press, San Diego, California, USA. 452 pp.

SHU F. H., SHANG H. AND LEE T. (1996) Toward an astrophysical theory of chondrites. *Science* **271**, 1545–1552.

SHU F. H., SHANG H., GOUNELLE M., GLASSGOLD A. E. AND LEE T. (2001) The origin of chondrules and refractory inclusions in chondritic meteorites. *Astrophys. J.* **548**, 1029–1050.

SORBY H. (1877) On the structure and origin of meteorites. *Nature* **15**, 495–498.

SPIEGEL E. A. (1972) Convection in stars. II. Special effects. *Ann. Rev. Astron. Astrophys.* **10**, 261–304.

STACEY F. D., LOVERING J. F. AND PARRY L. G. (1961) Thermomagnetic properties, natural magnetic moments and magnetic anisotropies of some chondritic meteorites. *J. Geophys. Res.* **66**, 1523–1534.

STOLPER E. AND PAQUE J. (1986) Crystallization sequences of Ca-Al-rich inclusions from Allende: An experimental study. *Geochim. Cosmochim. Acta* **50**, 1785–1806.

SUGIURA N., LANOIX M. AND STRANGWAY D. W. (1979) Magnetic fields of the solar nebula as recorded in chondrules from the Allende meteorite. *Phys. Earth Planet. Int.* **20**, 342–349.

SWINDLE T. D., DAVIS A. M., HOHENBERG C. M., MACPHERSON G. J. AND NYQUIST L. E. (1996) Formation times of chondrules and Ca-Al-rich inclusions: Constraints from short-lived radionuclides. In *Chondrules and the Protoplanetary Disk* (eds. R. H. Hewins, R. H. Jones and E. R. D. Scott), pp. 77–86. Cambridge Univ. Press, New York, New York, USA.

TANAKA K. K., TANAKA H., NAKAZAWA K. AND NAKAGAWA Y. (1998) Shock heating due to accretion of a clumpy cloud onto a protoplanetary disk. *Icarus* **134**, 137–154.

WASILEWSKI P. J. AND DICKINSON T. (1995) Interpretation of meteorite magnetic records needs a paradigm shift (abstract). *Meteoritics* **30**, 594.

WASILEWSKI P. J. AND DICKINSON T. (2000) Aspects of the validation of magnetic remanence in meteorites. *Meteorit. Planet. Sci.* **35**, 537–544.

WASILEWSKI P. J. AND O'BRYAN M. V. (1994) Chondrule magnetic properties (abstract). *Lunar Planet. Sci.* **25**, 1467–1468.

WASSON J. T. (1993) Constraints on chondrule origins. *Meteoritics* **28**,14–28.

WASSON J. T. (1996) Chondrule formation: Energetics and length scales. In *Chondrules and the Protoplanetary Disk* (eds. R. H. Hewins, R. H. Jones and E. R. D. Scott), pp. 45–54. Cambridge Univ. Press, New York, New York, USA.

WASSON J. T., KROT A. N., MIN S. L. AND RUBIN A. E. (1995) Compound chondrules. *Geochim. Cosmochim. Acta* **59**, 1847–1869.

WEIDENSCHILLING S. J., MARZARI F. J. AND HOOD L. L. (1998) The origin of chondrules at Jovian resonances. *Science* **279**, 681–684.

WEINBRUCH S. AND MULLER W. F. (1995) Constraints on the cooling rates of chondrules from the microstructure of clinopyroxene and plagioclase. *Geochim. Cosmochim. Acta* **59**, 3221–3230.

WEINBRUCH S., BUETTNER H., HOLZHEID A., ROSENHAUER M. AND HEWINS R. H. (1998) On the lower limit of chondrule cooling rates: The significance of iron loss in dynamic crystallization experiments. *Meteorit. Planet. Sci.* **33**, 65–74.

WESTPHAL M. AND WHITECHURCH H. (1983) Magnetic properties and paleointensity determination of seven H-group chondrites. *Phys. Earth Planet. Int.* **31**, 1–9.

WHIPPLE F. L. (1966) A suggestion as to the origin of chondrules (abstract). SAO special report #206. Smithsonian Astrophysical Observatory, Cambridge, Massachusetts, USA.

WOOD J. A. (1963) Chondrites and Chondrules. *Sci. Am.* **209**, 64–82.

WOOD J. A. (1984) On the formation of meteoritic chondrules by aerodynamic drag heating in the solar nebula. *Earth Planet. Sci. Lett.* **70**, 11–26.

WOOD J. A. (1985) Meteoritic constraints on processes in the solar nebula. In *Protostars and Planets II* (eds. D. C. Black and M. S. Matthews), pp. 687–702. Univ. Arizona Press, Tucson, Arizona, USA.

WOOD J. A. (1996) Processing of chondritic and planetary material in sprial density waves in the nebula. *Meteoritics* **31**, 641–645.

YU Y. AND HEWINS R. H. (1998) Transient heating and chondrule formation: Evidence from sodium loss in flash heating simulation experiments. *Geochim. Cosmochim. Acta* **62**, 159–172.

YU Y., HEWINS R. H. AND ZANDA B. (1996) Sodium and sulfur in chondrules: Heating time and cooling curves. In *Chondrules and the Protoplanetary Disk* (eds. R. H. Hewins, R. H. Jones and E. R. D. Scott), pp. 213–220. Cambridge Univ. Press, New York, New York, USA.

ZINNER E. (1997) Presolar material in meteorites: An overview. In *Astrophysical Implications of the Laboratory Study of Presolar Materials* (eds. T. J. Bernatowicz and E. Zinner), p. 3. American Institute of Physics, Woodbury, New York, USA.

APPENDIX A

Gas-Solid Transfers

The drag force, the rate at which momentum is transferred from the gas to dust grains, has been calculated by Probstein (1968) in the limit that gas atoms and molecules are thermally accomodated (brought to the solid's temperature) before leaving the solid's surface, and that the gas atoms and molecules are reflected diffusively. The mean molecular flow approximation can be used if the particle radius a_j is smaller than the mean free path λ of the gas atoms and molecules, $a_j < 2.25/(n\sigma)$ (Cuzzi *et al.*, 1996). Using a cross section $\sigma \approx 5 \times 10^{-16}$ cm^2, and a particle diameter of 1 mm leads to an upper limit to the density n to which this approximation is valid, $\sim 10^{17}$ cm^{-3}, or $\rho_g \approx 3 \times 10^{-7}$ g cm^{-3}. For valid densities, the drag force is given by Eq. (11), with a drag coefficient

$$C_D = \frac{2}{3s}\left(\frac{\pi T_j}{T_g}\right)^{1/2} + \frac{2s^2+1}{\pi^{1/2}s^3}\exp\left(-s^2\right) + \frac{4s^4+4s^2-1}{2s^4}\mathrm{erf}(s) \quad \text{(A1)}$$

Here T_j is the solid's temperature, T_g is the gas temperature, and

$$s = \frac{\left|V_j - V_g\right|}{(2kT_g/\bar{m})^{1/2}} \quad \text{(A2)}$$

$\bar{m}$ being the mean molecular weight of the gas species and k the Boltzmann constant. In the limit $s >> 1$, $C_D \to 2$, while in the limit $s << 1$, $C_D \to (2/3s)(\pi T_j/T_g)^{1/2}$. In practice, a different coefficient C_D exists for each of the four gas species considered.

The heating rate of particles by the gas, due to frictional heating or thermal exchange, is Eq. (12), with different parameters T_{rec} C_H defined for each gas species:

$$T_{rec} = T_{gas}\left(\frac{\gamma-1}{\gamma+1}\right)\left[\frac{2\gamma}{\gamma-1} + 2s^2 - \left(\frac{1}{2} + s^2 + \frac{s}{\pi^{1/2}}\exp\left(-s^2\right)\mathrm{erf}^{-1}(s)\right)^{-1}\right] \quad \text{(A3)}$$

and

$$C_H = \frac{\gamma+1}{\gamma-1}\frac{k}{8\bar{m}s^2}\left[\frac{s}{\pi^{1/2}}\exp\left(-s^2\right) + \left(\frac{1}{2}+s^2\right)\mathrm{erf}(s)\right] \quad \text{(A4)}$$

The same gas temperature T_{gas} is used for each species, but $\gamma = 7/5$ for H_2 and SiO and $\gamma = 5/3$ for H and He, and s will be different for each species as well, since $\bar{m} = 1m_H$ for H, $2m_H$ for H_2, $4m_H$ for He, and $44m_H$ for SiO. In the limit that $s << 1$, $T_{rec} \to T_g$ and $C_H \to [(\gamma+1)/(\gamma-1)]\,[k/(4\pi^{1/2}\bar{m}s)]$, while in the limit $s >> 1$, $T_{rec} \to 2[(\gamma-1)/(\gamma+1)]s^2T_{gas}$ and $C_H \to [(\gamma+1)/(\gamma-1)]\,(k/8\bar{m})$. Altogether, if $s >> 1$, gas-drag heating dominates over thermal exchange and the heat flux is

$$q \to \frac{1}{8}\rho_{gas}\left|V_j - V_g\right|^3 \quad \text{(A5)}$$

In the opposite limit, when $s << 1$ and thermal exchange dominates over gas-drag heating,

$$q \rightarrow \left(\frac{\rho_g}{\bar{m}}\right)\frac{1}{4}\left(\frac{8kT_g}{\pi\bar{m}}\right)^{1/2}\frac{1}{2}\left(\frac{\gamma+1}{\gamma-1}\right)k\left(T_g - T_j\right) \quad \text{(A6)}$$

APPENDIX B

Dissociation and Recombination

In the gas phase, H atoms can combine to form H_2 molecules. Because H_2 is a nonpolar molecule, it cannot radiate away the excess chemical energy of formation by allowed transitions, and H_2 formation must proceed by three-body reactions, with either H atoms or H_2 molecules as the catalysts. Once formed, H_2 molecules are dissociated by collisions with H atoms or other H_2 molecules. The net rate at which H atoms recombine in the gas phase is (Cherchneff *et al.*, 1992):

$$R = +n_H^2\left(a_1 n_{H_2} + a_2 n_H\right) - n_{H_2}\left(a_3 n_{H_2} + a_4 n_H\right) \quad \text{(B1)}$$

$$a_1 = 8.72 \times 10^{-33}\left(\frac{T_g}{300\ \text{K}}\right)^{-0.6}\ \text{cm}^6\ \text{s}^{-1} \quad \text{(B2)}$$

$$a_2 = 1.83 \times 10^{-31}\left(\frac{T_g}{300\ \text{K}}\right)^{-1}\ \text{cm}^6\ \text{s}^{-1} \quad \text{(B3)}$$

$$a_3 = 1.50 \times 10^{-9}\ \exp\left(-\frac{46350\ \text{K}}{T_g}\right)\text{cm}^3\ \text{s}^{-1} \quad \text{(B4)}$$

$$a_4 = 3.75 \times 10^{-8}\left(\frac{T_g}{300\ \text{K}}\right)^{-0.5}\exp\left(-\frac{53280\ \text{K}}{T_g}\right)\text{cm}^3\ \text{s}^{-1} \quad \text{(B5)}$$